OPTICS OF INSTANTANEOUS WAVES

Alexandr B. Shvartsburg, Guillaume Petite

OPTICS OF INSTANTANEOUS WAVES

By

Alexander B. SHVARTSBURG

Central Design Bureau for Unique Instrumentation of the RAS

Butlerov Str. 15, Moscow, Russia

and

Guillaume PETITE

Laboratoire des Solides Irradiés, CEA/DSM/DRECAM, CNRS (UMR 7642)

and Ecole Polytechnique, 91128, Palaiseau, France

to be published in :"Progress in Optics"

OUTLINE

ABSTRACT

This review is devoted to the transient optical phenomena, displayed both in the spatiotemporal dynamics of ultrashort single - cycle wave pulses in free space and dispersive dielectrics as well as to interaction of light with non-stationary media. The interplay of diffractive and dispersive phenomena, including the coupled processes of amplitude and phase reshaping, spectral variations, polarity reversal for different types of light pulses, is examined in frequency and time domains. Reflection - refraction effects on the interfaces of media with time-dependent dielectric susceptibility are considered by means of exact analytical solutions of Maxwell equations for these media. The non - stationarity - induced dispersion is shown to provide a dynamical regime of reflectivity of non-stationary media, depending upon both instantaneous dielectric susceptibility and its temporal derivative; the relevant generalization of Fresnel formulae is presented

INTRODUCTION :

This paper is devoted to the physical fundamentals and mathematical basis of the optics of waveforms whose parameters vary in the course of propagation. The dynamics of instantaneous optical fields, travelling in free space and continuous media, opens many new opportunities for controlled spatio-temporal reshaping of these fields. The ongoing interest towards such problems in fueled by several research goals:

- to optimize the processes of light pulses transfer through optical systems; this is particularly important in view of the applications to optical communication : the use of ultrashort pulses at high repetition rate is one of the approaches to the increase of the transfer rate.
- to develop methods of fast non-destructive testing of materials and targets, atmospheric sensing, using ultrashort broadband electromagnetic (EM) pulses;
- to reach a comprehensive understanding of such ultrafast processes as amplitude or phase modulation of EM waves interacting with non stationary media.

Moreover, an important task is to elaborate an analytical approach to these topics, which were considered until recently as an exclusive field of computer simulations.

The investigation of coupled processes of spatial and temporal deformations of localized waveforms is preceded here by a brief description of waveforms widely used in modeling of such processes. Both frequency and time-domain models are presented below in Section I-1. We then briefly recall how such waveforms are produced (I-2), and measured experimentally (I-3).

Two opposite statements of the problems of instantaneous optics will then be treated. Section II is focused on the spatio-temporal dynamics of localized EM pulses interacting with stationary dielectric media. On the contrary, the reshaping of harmonic CW trains interacting with non-stationary media is discussed in Section III. In this latter case, a special attention will be given to some exactly solvable models, providing a better physical insight into these problems.

I. ULTRASHORT EM PULSES : HOW THEY ARE MODELED, PRODUCED, MEASURED.

It is first necessary to agree upon what will be defined as an ultrashort electromagnetic pulse. Here we will retain the following definition : a pulse whose duration is of the order of a few, at most a few tens of periods of the EM field. It is of course almost equivalent to consider pulses whose spectral width is a substantial fraction of their frequency, except that one rather adresses in this case the coherence length of the pulse than its duration, so that this definition would be strictly valid for radiation presenting complete temporal coherence only, a criterion which is not even satisfied by all lasers. In this section, we will first recall some of the mathematical models which have been used to represent such pulses (§ I.1), and we will then briefly recall how such pulses are produced (§ I.2) and measured (§ I.3).

I.1) Non-Sinusoidal Waveforms of Electromagnetic Waves.

Let us begin this analysis from the traditional spectral approach. To optimize a waveform $E(t) = E_0 F(t)$ with respect to a bandwidth-limited communication system or to the width of an absorption line, it is traditional to work with its Fourier transform (FT). Some properties of waveforms $F(t)$, having an essential influence on their spectral bandwidths, such as their duration and rise time, are considered below.

I.1.1. Square-shaped truncated train of monochromatic waves, are represented by the function :

$$F(t) = \begin{cases} \cos(\omega_0 t)\ ;\ |t| \le |t_0| \\ \\ 0\ ;\qquad |t| > |t_0| \end{cases} \tag{1.1}$$

The FT of this waveform is known to be

$$F_\omega(\omega) = \frac{\sin[t_0(\omega_0 - \omega)]}{\omega_0 - \omega} \tag{1.2}$$

The spectral density of EM energy $\mathrm{E}(\Delta)$ in a pulse F (1.1), localized in some finite spectral range ($\omega \pm \Delta/2$), writes

$$\mathrm{E}(\Delta) = |E_0|^2 W(\Delta) \; ; \; W(\Delta) = \frac{1}{2\pi} \int_{\omega_0 - \Delta/2}^{\omega_0 + \Delta/2} |F_\omega|^2 \, d\omega \tag{1.3}$$

The spectral density E calculated for an infinite spectral range, $\Delta \to \infty$, is given by the function W(∞). The spectral bandwidth of a pulse is defined as the range of frequencies $\omega_0 \pm \Delta$, containing some given fraction δ (e.g., δ = 90% or 99%) of the pulse energy

$$W(\Delta) = \delta \times W(\infty) \tag{1.4}$$

Substituting the Fourier amplitude F_ω (1.2) into (1.3) and introducing a variable $x = t_0 \Delta$ we obtain the function $W(\Delta)$

$$W(\Delta) = \frac{t_0}{2\pi} \left[Si(2x) - \frac{\sin^2 x}{x} \right] \tag{1.5}$$

where $Si(x)$ is the integral sine function

$$Si(x) = \int_0^x \frac{\sin y}{y} dy \tag{1.6}$$

Using the value $Si(\infty) = \pi/2$, one can present eq. (1.4), governing the value of spectral-time product $K_c = t_0 \Delta_c$, in a form

$$Si(2K_c) - \frac{\sin^2 K_c}{K_c} = \frac{\pi}{2} \delta \tag{1.7}$$

Considering the central part of the distribution F_ω (1.2), located between the zeros of F_ω ($K_c = \pm\pi$), one can see that 90% of the pulse energy is contained in the spectral range $\omega_0 \pm \pi/t_0$. Any further significant growth of this fraction δ requires a substantial increase of spectral range : for δ = 0.99, the spectral range K_c is increasing by more than a factor 10.

It is worthwhile to compare the broadband square-shaped pulses, characterized by a short rise time, tending formally towards zero, with other waveforms possessing the same characteristic duration, but a finite risetime.

I.1.2. To illustrate the influence of increasing rise- and falltime, let us consider the Gaussian-shaped waveform

$$F(t)=\exp\left(-\frac{t^2}{2t_0^2}\right) \tag{1.8}$$

the FT of a Gaussian waveform is known to be also Gaussian

$$F_\omega = t_0\sqrt{2\pi}\exp\left[-\frac{(\omega t_0)^2}{2}\right] \tag{1.9}$$

It is often convenient to characterize the pulse by its full width at half-maximum (FWHM). The Gaussian waveform (1.8) and its FT (1.9) are defined by the FWHM values t_c and ω_c

$$t_c = 2.35t_0 \quad ; \quad \omega_c = \frac{2.35}{t_0} \quad ; \quad t_c\omega_c = 5.55 \tag{1.10}$$

Using the first of relations (1.10), one can present the Gaussian profile (1.8) in a form, expressed via the FWHM

$$F(t)=\exp\left(-\left[\frac{1.67t}{t_c}\right]^2\right) \tag{1.11}$$

Calculating the function $W(\Delta)$ (1.3), related to the FT (1.9), we obtain the equation, governing the bandwidth Δ_c

$$erf(t_0\Delta_c)=\delta \tag{1.12}$$

Here *erf* is the error function. Taking, e.g., δ=0.9, one has $K_c=t_0\Delta_c$=1.17, and thus the bandwidth Δ_c of the Gaussian pulse (1.8) is almost three times smaller than that of the square-shaped pulse ($K_c=\pi$ for δ=0.9). This example shows that an increase of rise time, the pulse duration being fixed, induces a strong spectral narrowing.

Some pulses with extremely steep leading edges have been proposed as prospective carriers for directed energy transmission in free space. Such a pulse, entitled by Wu [1985] "electromagnetic missile", yields a diffracted wave decaying slower than z^{-2} in intensity. Considering a broadband pulse passing through a plane circular aperture with radius a, one can

see that the boundaries of the first Fresnel zone $z_F=\omega a^2c^{-1}$ for high frequencies ω become extremely distant. Wu [1985] showed that when the pulse spectrum is damping slowly in the high-frequency limit $\omega\to\infty$, even though the energy collected on a detector of finite dimensions is still tending to zero when $z\to\infty$, it can be made to do so in an arbitrarily slow manner. An example of such pulses is expressed as a function of time via the modified Bessel function K_ν of ν-th order:

$$F(t)=\left(\frac{t}{t_0}\right)^{\nu}K_\nu\left(\frac{t}{t_0}\right) \tag{1.13}$$

Taking the cosine FT from (1.13), we obtain

$$F_\omega=\frac{\sqrt{\pi}\,2^{\nu-1}t_0\Gamma\left(\nu+\frac{1}{2}\right)}{\left(1+\omega_0^2t_0^2\right)^{\nu+\frac{1}{2}}} \tag{1.14}$$

Presenting ν in a form $\nu=-\frac{1}{2}+\gamma;\ \gamma>0$, one finds as asymptotic spectral behavior of $F_\omega\big|_{\omega\to\infty}\approx\omega^{-2\gamma}$; thus, following Wu [1985], an appropriate choice of parameter γ yields an arbitrarily slow decrease of the high-frequency limit of (1.14), providing a weakened angular divergence of the pulse at distances $z\geq\omega a^2c^{-1}$.

I.1.3. Until now we have discussed ways to broaden or to narrow the spectral bandwidths for waveforms of a given duration $2t_0$. Steepening of the pulse fronts was shown to cause an increase of the spectral bandwidth; their softening can give rise to a narrowing of the spectrum. However, it should be mentioned that there is an implicit simplification in all the above developments, which is that we have not allowed statistical fluctuations between the different spectral components of the EM field we studied. Any classical source will present such fluctuations, as well as most of the lasers. All the above developments thus deal with temporally coherent sources such as single longitudinal mode or mode-locked lasers. One often refers to such pulses as “Fourier Transform limited pulse” (in the sense that the bandwith of a partially coherent pulse

will be larger than strictly required by the FT). It should be mentioned that there is a stricter definition of a FT-limited pulse, which is the one having the narrowest pulse width possible for a given spectral amplitude distribution. The term "amplitude" may be misleading here since the spectral amplitudes are in reality complex, and the actual temporal shape of the pulse will depend on the shape of the "spectral phase" $\varphi(\omega)$. Fig. 1 illustrates this point by comparing two pulses having the same power spectrum ($|f(\omega)|^2$), but different spectral phase behaviors. It shows that the pulse with the minimum width (and in this sense, strictly speaking FT-limited) is the one presenting a linear spectral phase frequency dependence.

The physical and computational problems, resulting from the efforts to adjust the Fourier "ω-k" language to the dynamics of ultrashort waveforms in dispersive media, stimulated the development of time-domain models, i.e. directly using the temporal dependence of electric and magnetic strength of EM field, for such waveforms.

I.1.4. Models of pulses assuming equality of rise and fall times have been considered so far. However, there are many real optical pulses that do not have such symmetry. An example of strongly asymmetrical waveform, described by a Gaussian rising edge, followed by an exponentially falling tail

$$E(t)=\begin{cases} E_0 \exp\left[-\left(\dfrac{1.67t}{t_C}\right)^2\right]; & t\le 0 \\ E_0 \exp\left(-\dfrac{t}{t_0}\right); & t\ge 0 \end{cases} \qquad (1.15)$$

was discussed by Qian and Yamashita (1992). This so-called single-cycle exponential waveform has a discontinuity of derivative at the maximum t = 0. A double- exponential waveform, posessing a continuous derivative at the maximum :

$$E(t) = E_0\left[\exp\left(-\frac{t}{t_1}\right) - \exp\left(-\frac{t}{t_2}\right)\right] \tag{1.16}$$

was used by Ma and Ciric [1992] for the analysis of transient scattering on small targets; in the case ($t_1 >> t_2$), profile (1.16) resembles a single-sided waveform, but differs from (1.15) by a smooth maximum.

Flexible models, describing continuous waveforms with an arbitrary amount of different extrema and unequal distances between zero-crossing points, were used in time-domain optics by Shvartsburg [1999]. These waveforms, characterized by well-expressed leading fronts with finite slope, an arbitrary number of unharmonic oscillations and exponentially damping tails, are defined by the series of Laguerre functions L_n in the time interval $0 \le t < \infty$

$$E(t) = \sum_{n=0}^{\infty} a_n L_n\left(\frac{t}{t_0}\right) \tag{1.17}$$

The Laguerre functions (Fig. 2)

$$L_n(x) = \frac{\exp\left(-\frac{x}{2}\right)}{n!}\frac{d^n}{dx^n}\left[x^n \exp(-x)\right] \tag{1.18}$$

are known to be orthonormal in the interval $0 \le x \le \infty$, that is to say :

$$\int_0^{\infty} L_n(x) L_m(x) dx = \delta_{nm} \tag{1.19}$$

These waveforms, localized in time, are suitable for description of plane wave pulses. However, to consider the dynamics of both spatially and temporally localized fields, other families of waveforms are needed.

I.1.5. The spatiotemporal structure of few-cycle three-dimensional pulsed wave beams can be described by means of so-called Poisson-spectrum pulses

$$F(t) = \Re ef(t) \quad ; \quad f(t) = \left(\frac{it_0}{t' + it_0}\right)^m \tag{1.20}$$

Here $\Re ef$ indicates the real part of the function $f(t)$; $t_0>0$ and $m\geq 1$ are free parameters, t' is the retarded time for points located on the beam axis $t' = t - zc^{-1}$. This model, discussed by Porras [1998], is suitable for presentation of waveforms of any duration and with an arbitrary number of oscillations (Fig. 3). The FT of waveform (1.20) gives the Poisson spectrum, also called the power spectrum

$$F_\omega = \frac{\pi t_0^m |\omega|^{m-1}}{\Gamma(m)} \exp\left(-|\omega| t_0\right) \tag{1.21}$$

Unlike the above mentioned waveforms, the function F (1.20) can be used for modeling of spatio-temporal evolution of narrow directed pulsed beams with curvilinear wave fronts. To describe the non-stationary three-dimensional structure of such beams one has to replace the retarded time t' by the shifted time $t' - r^2/2cR$; where R and r are the radius of wave front curvature and the distance between the beam's axis and the observation point on the wave front. This non-separable waveform, containing both temporal and spatial variables, provides a useful analytical tool for investigation of coupled diffraction and dispersion- induced distortions of localized fields.

The spatiotemporal dynamics of all the aforesaid waveforms has to be investigated by means of relevant solutions of Maxwell equations. On the contrary, some localized waveforms, which are packet – like solutions of Maxwell equations in a free space themselves, are recalled below.

I.1.6. Search of packet-like solutions of the wave equation in free space

$$\frac{\partial^2 U}{\partial x^2} + \frac{\partial^2 U}{\partial y^2} + \frac{\partial^2 U}{\partial z^2} - \frac{1}{c^2}\frac{\partial^2 U}{\partial t^2} = 0 \tag{1.22}$$

led to the following family of solutions, presented by Bateman [1955] in a form

$$U(\mathbf{r},t) = g(\mathbf{r},t) f(\theta) \tag{1.23}$$

Here $\mathbf{r}$ stands for the spatial variables, $\theta = \theta(\mathbf{r},t)$ is a solution of eikonal equation

$$\left(\frac{\partial\theta}{\partial x}\right)^2+\left(\frac{\partial\theta}{\partial y}\right)^2+\left(\frac{\partial\theta}{\partial z}\right)^2-\frac{1}{c^2}\left(\frac{\partial\theta}{\partial t}\right)^2=0 \tag{1.24}$$

and f is an arbitrary function. Two simple examples of waveform-preserving solutions (1.23) are (a) plane waves : $\theta = z - ct$, (b) spherical waves : $\theta = R - ct$. A third class of solutions (1.23), reported by Hillion [1983], is based on :

$$\theta = z - ct + \frac{r^2}{z + ct - ib} \tag{1.25}$$

Here b is an arbitrary positive constant, having the dimension of a length. Making use of (1.25) one can express the solution U of wave equation (1.23) via an arbitrary function $f(\theta)$

$$U = \frac{f(\theta)}{z + ct - ib} \tag{1.26}$$

The free choice of function $f(\theta)$ provides a remarkable flexibility in the modeling of localized fields. For instance, in a case considered by Brittingham [1983], $f(\theta)$ was chosen as

$$f(\theta) = \exp(iK\theta) \tag{1.27}$$

where K is a free real parameter. Separation of real and imaginary parts in (1.27) permits to separate the amplitude and phase factors in the field presentation (1.26)

$$U_1 = \frac{\exp\left(-\frac{r^2}{l_\perp^2}\right)}{\sqrt{(z+ct)^2+b^2}}\exp\left\{-i\left[K(z-ct)+\frac{b}{z+ct}+\frac{z+ct}{b}\frac{r^2}{l_\perp^2}\right]\right\} \tag{1.28}$$

This field is localized around the direction of propagation (z – axis) as a Gaussian – like pulse with the transversal width

$$l_\perp = \sqrt{\frac{(z+ct)^2+b^2}{Kb}} \tag{1.29}$$

However, the energy of the pulse (1.28) happens to be infinite, but this approach gave rise to forthcoming improvements of such packet - like solutions, providing them a finite energy. Indeed, taking the function $f(\theta)$ in a form

$$f(\theta)=\exp\left[2Kb\left(1-\sqrt{1-\frac{i\theta}{b}}\right)\right] \tag{1.30}$$

Kiselev and Perel (2000) demonstrated the packet – like behavior of solution (1.26) near by the point r=0, z=ct, θ=0. This point is viewed as the center of the packet, moving along the z -axis with velocity c. Expansion of the function f (1.30) in the vicinity of this point in a case Kb >>1, brings about the approximation

$$U_2=U_1\exp\left[-\frac{(z-ct)^2}{l_{//}^2}\right] \quad ; \quad l_{//}=\sqrt{\frac{b}{K}} \tag{1.31}$$

Substitution of (1.31) into (1.26) yields the representation of the field near its peak in a form differing only from solution U_1 (1.28) by an exponential factor, providing longitudinal localization

$$U_2=U_1\exp\left[-\frac{(z-ct)^2}{l_{//}^2}\right] \tag{1.32}$$

Expression (1.32) describes a wave packet, filled with non-sinusoidal oscillations; its envelope decreases in a Gaussian-like manner, both in longitudinal and transversal directions. Unlike the pulse U_1 , the energy of waveform U_2 is finite.

I.1.7. - New types of waveforms presenting non-separable solutions to the propagation of a pulse of EM field in a collisionless plasma, characterized by its "plasma frequency" Ω, such that $\Omega^2=4\pi Ne^2/m$ (N,e and m are the electron density, charge and mass respectively) have been suggested by Shvartsburg [1999]. Starting with the vector potential of the field $A(A_x,0,0)$ such that

$$E_x=-\frac{1}{c}\frac{\partial A_x}{\partial t} \quad ; \quad H_y=\frac{\partial A_x}{\partial z} \tag{1.33}$$

Substitution of (1.33) into the Maxwell equations yields the propagation equation, governing the vector-potential

$$\frac{\partial^2 A_x}{\partial z^2}-\frac{1}{c^2}\frac{\partial^2 A_x}{\partial t^2}=\frac{\Omega^2}{c^2}A_x \tag{1.34}$$

The traditional solution of eq. (1.34) takes the form of harmonic wave trains : $A_x = A_0 \exp[i(kz - \omega t)]$. In such a case the wave number k and the frequency ω are linked by the dispersion equation, derived from (1.34)

$$k^2 c^2 = \omega^2 - \Omega^2 \tag{1.35}$$

However, side by side with these sinusoidal wave trains, there is a huge family of exact non-sinusoidal solutions of eq. (1.34). To analyze the spatiotemporal structure of such anharmonic EM fields in plasma, it is convenient to introduce the normalized variables τ and η and the dimensionless function f

$$\tau = \Omega t \quad ; \quad \eta = \frac{\Omega z}{c} \quad ; \quad f = A_x A_0^{-1} \tag{1.36}$$

Making use of (1.36), one can rewrite eq. (1.34) in a dimensionless form

$$\frac{\partial^2 f}{\partial \eta^2} - \frac{\partial^2 f}{\partial \tau^2} = f \tag{1.37}$$

(1.37) is the Klein-Gordon (KG) equation. Solutions of this equation, suitable for time-domain optics, were presented by Shvartsburg [1999] in a form:

$$f = \sum_{q=q_0}^{\infty} d_q f_q(\tau, \eta) \tag{1.38}$$

$$f_q(\tau, \eta) = \frac{1}{2}\left[\psi_{q-1}(\tau, \eta) - \psi_{q+1}(\tau, \eta)\right] \tag{1.39}$$

$$\psi_q(\tau, \eta) = \left(\frac{\tau - \eta}{\tau + \eta}\right)^{q/2} J_q\left(\sqrt{(\tau^2 - \eta^2)}\right) \tag{1.40}$$

Here J_q is the Bessel function of order q; the coefficients d_q and the values q will be determined from the continuity conditions on the boundary plane η. The non-separable functions ψ_q cannot be written in the usual form of a product of time-dependent and coordinate-dependent factors. Let us point out some of their salient features:

(i). They have both spatial and temporal derivatives of arbitrary orders, which may be calculated by means of recursive formulae:

$$\frac{\partial \psi_q}{\partial \tau} = \frac{1}{2}\left(\psi_{q-1} - \psi_{q+1}\right) \tag{1.41}$$

$$\frac{\partial \psi_q}{\partial \eta} = -\frac{1}{2}\left(\psi_{q-1} + \psi_{q+1}\right) \tag{1.42}$$

(ii). The causal condition $\tau \geq \eta$, which is fulfilled for each observation point $\eta \geq 0$, results in restriction of the magnitudes of harmonics ψ_q for $q \geq 0$. The function ψ_q on a plane $\eta=0$ reduces to

$$\psi_q\big|_{\eta=0} = J_q(\tau) \tag{1.43}$$

(iii). The electric and magnetic components of the EM field are also presented by non-separable harmonics. Using (1.33), we obtain

$$E_x(\tau,\eta) = -\frac{A_0\Omega}{c}\sum_{q=q_0}^{\infty} d_q e_q(\tau,\eta);\; H_y(\tau,\eta) = -\frac{A_0\Omega}{c}\sum_{q=q_0}^{\infty} d_q h_q(\tau,\eta) \tag{1.44}$$

$$e_q(\tau,\eta) = \frac{1}{4}\left(\psi_{q-2} - 2\psi_q + \psi_{q+2}\right) \tag{1.45}$$

$$h_q(\tau,\eta) = \frac{1}{4}\left(\psi_{q-2} - \psi_{q+2}\right) \tag{1.46}$$

Examples of electric and magnetic harmonics with $q=3$ are depicted on Fig. 4. One can see that these harmonics are non-sinusoidal, non-stationary and that their spatiotemporal structures are quite different.

The models of localized pulses discussed above are far from exhausting the huge variety of non-sinusoidal waveforms, and were chosen since they will be exploited in Section II.

I.2 : Production of ultrashort EM pulses

Production of such ultrashort EM pulses started long before the lasers were even thought of, with the advent a long time ago of short pulse radars. We will not address this point here, and rather concentrate on the production of short optical pulses, and some of their derivatives. Techniques consisting in optically gating a cw laser have been developed but they do not, so far, give access to pulse durations below 1 ps, and thus do not really satisfy the above definition. As

can be immedialtely deduced from the statement made above that short pulses have broad spectra, production of short laser pulses requires either materials that can support a large gain bandwidth, or to develop techniques to increase, in the course of propagation, the spectrum of the pulse, which therefore pertain to non-linear optics. Obviously, the same materials used for broadband tuneability can in principle be used for production of ultrashort laser pulses. Indeed, dye lasers were the first to allow, more than twenty years ago, production of pulses whose duration were significantly below 10^{-13} s. However, it is fair to say that in the past ten years, all-solid state systems have definitely outruned dye-based systems in the race for production of high intensity ultrashort pulses. Several materials have been considered for such applications, including alexandrite, LiSAF crystals, and titanium doped sapphire (ti:sa), definitely the most commonly used nowadays because of its excellent thermal and spectral qualities, and particular non-linear properties offering the opportunity of a simple mode-locking mechanism. With a central wavelength in the near IR, a spectral bandwidth in the 100 nm range, one can expect pulse durations in the 10 fs range. Three essential functions have to be realized in such a laser :

- broadband amplification, which is provided by the amplifying material
- mode-locking, which is based in such lasers on the “Kerr-lens mode locking” mechanism.

Because of the high intensities reached at the focus of the Z-shaped subcavity, where the amplifying crystal is located, non-linear contributions to the index of the material’s refractive index (Kerr effect) cause the appearance of a “Kerr lens” instead of the parallel slab used, which in turn perturbs the cavity stability. This effect can be corrected by a readjustment of the Z-shaped subcavity mirrors, with the consequence that the total cavity is now optimized for the high intensity (pulsed) regime. Besides, it is possible to select the spatial modes corresponding to a pulsed operation using a slit conveniently placed in the oscillator cavity. It is worth noting that, if one considers a pulse travelling back and forth in the cavity, the gain perturbation caused by the appearance of the Kerr effect occurs everytime the pulse passes in the amplifying crystal, i.e. perturbation of the gain occurs at the intermode frequency, a known condition for obtaining

mode-locked operation of a laser. This self-modelocking effect (once known as “magic” modelocking!) was essential in the success of such lasers.

- Compensation of the Group-Velocity Dispersion (GVD) induced both in the amplifying crystal and also, to some extent, in the coatings used for the different mirrors included in the cavity. This function is provided by a “negative dispersion line”, usually consisting of two identical isoscele prisms placed in one of the arms of the cavity.

With such oscillators, one now currently obtains pulses with duration in the 10 to 20 fs range, with energies of 1 nJ or more, i.e. peak power in excess of a GigaWatt, making non linear optics experiments accessible in quite confortable conditions. It should be mentioned that the world record for pulse duration in such systems (5.8 fs, Matuschek, Gallmann, Sutter Steinmeyer and Keller [2000]) was obtained using a different GVD principle, based on the use of “chirped mirrors” proposed by Szipöcs, Ferencz, Spielman and Krausz [1995]. This solution, now commercially available, also offers excellent compactness and stability. Note that for such short time durations, the natural bandwidth of the amplifying material is not sufficient. It is Self Phase Modulation in the amplifying crystal (a temporal counterpart of the Kerr effect) which provides the extra bandwith needed.

Amplification of such laser pulses in solid-state amplifiers was the occasion of another revolution, with the appearance of the “Chirped Pulse Amplification” technique (Maine, Strickland, Badot, Pessot and Mourou, [1988]) –first applied to Table-Top Terawatt (T^3) neodymium lasers – which will not be detailed here. Let us just mention that it relies on a three stage manipulation of the pulse : stretching of the ultrashort pulse to nanosecond durations, amplification (which under these conditions can extract efficiently the energy stored in the amplifiers material without reaching the material breakdown threshold) and recompression of the pulse almost to its original duration. Pulses of typically 25 fs/25 J can be produced this way in the most advanced ti:sa systems, allowing to reach intensities in excess of $10^{20}W.cm^{-2}$.

At much lower intensities (typically 10^{14} W.cm^{-2}), interaction with dense gaseous targets allows to produce with a rather high efficiency a large number of odd harmonics of the incident frequency (Salières, L'Huillier, Antoine and Lewenstein, [1999]). A typical harmonic spectrum generated in such interactions is shown on Fig. 5, which shows a case where both the fundamental beam and its second harmonic have been focused simultaneously to generate a complete spectrum (odd an even harmonics : the fundamental alone generates only odd harmonics). It has a very typical shape, consisting in a rather fast decrease of efficiency for the lowest order harmonics, followed by a "plateau" whose width and height depends on the gas used (rare gases, most often), and finally a cut-off region. The emitted harmonics have excellent spatial and temporal coherence properties, thanks to the coherent nature of the process producing them, and pulse duration smaller than that of the exiting laser. The number of photons per harmonic pulses is quite high (typically 10^8 in a common case where one does not seek to produce the shortest possible wavelength), and such sources, in some applications requiring short UV pulses are a serious competitor to synchrotron radiation (which is still leading the race, though, in terms of average power). Concerning the shortest wavelength that can be generated with such techniques, the latest results showed evidence of generation of the 255th harmonic of the ti:sa laser, i.e. a wavelength close to 3nm !

The particular shape of the spectrum shown on Fig. 5 has suggested a possible way of reducing the pulse duration of such harmonic far below 1 fs. If one could lock the phases between the different harmonics in the plateau region, modelisation predicts that pulse durations in the range of a few attoseconds (one attosecond equals 10^{-18} s) could be obtained. Very recently, the relative phase of the different harmonics were measured using a two photon IR-VUV ionization experiment (Paul, Toma, Breger, Mullot, Augé, Balcou, Muller and Agostini, [2001]), which allowed to reconstruct the harmonic pulse train, arriving to the conclusion that one individual harmonic pulse had a maximum duration of 250 as, the shortest EM pulse produced to date.

The search for ultrashort pulses has also been successful in the IR range. It has been known for some times that IR free electron lasers produce, in the leading edge of the "macropulse" (a train of 100 or more micropulses with picosecond or less duration) characteristic of such machines, pulses with durations of typically one picosecond, which, given the wavelength range considered (10 μm or more) satisfies the definition given above. Such lasers now almost routinely operate between 5 and 50 μm.

In the communication domain, lots of efforts have also been made to develop very high repetition rate-ultrashort optical sources. Usually starting from semiconductor lasers for compactness and cost efficiency reasons, such sources are based on compression techniques using propagation in different optical fibers. Limited for some times to the ps duration regime, recent progresses have allowed to obtain compression levels down into the 20 fs range, that is to say equivalent to that of the ti:sa lasers described above. In particular, starting from a 7.5-ps pulses generated from a gain-switched semiconductor laser at (λ=1.55 μm, rep. Rate 2 GHz), Matsui, Pelusi and Suzuki [1999] achieved their compression down to 20 fs using a four-stage fiber soliton pulse compressor consisting of standard single-mode transmission, Er-doped, dispersion-decreasing, and dispersion-flattened fibers, respectively. They confirmed experimentally that the soliton self-frequency shift plays an important role in obtaining such high compression in very short fibers, and also in minimizing the inherent undesirable pedestal component.

Finally, let us mention that the ultrashort laser pulses discussed above have been used to generate single or half-cycle Terahertz pulses. The principle of the experiment is the following : a piece of semi-conductor is irradiated during a short time using a subpicosecond laser pulse (You, Jones, Bucksbaum and Dykaar [1993]). The carriers injected in the sc thus allow a current to circulate in the sc, biased under a high dc voltage, as long as it is maintained in the conducting state by the laser illumination. The field radiated by the moving electrons has the temporal shape close to a single arch, and can be modeled as ½ cycle pulse of a radiation whose frequency is

determined by the illumination laser pulse duration, and falls in the Terahertz range. More recently this technique has been refined and THz emission obtained from unbiased GaAs (Code, Fraser, De-Camp, Bucksbaum and van Driel [1999]), originating from ballistic photocurrents generated via quantum interference of one- and two-photon absorption in low-temperature-grown and semi-insulating GaAs. At a 250 kHz repetition rate, up to 3 nW of THz power have been measured.

The examples given above show that it is possible, using the different techniques briefly summarized here, to obtain ultrashort EM pulses at almost any wavelength between milimeters (at least hundreds of μm) and nanometers.

I.3 – Measurement of ultrashort EM pulses.

Another problem is to measure such ultrashort EM pulses. If one excepts the case of ultrashort RF pulses, which can be measured using standard electronic techniques, no electronic equipment possesses a sufficient bandwidth to allow direct measurement of any, e.g., subpicoscond optical pulses. Therefore a number of optical techniques were proposed, and some of them are routinely in use, for measurement of not only the pulse duration, but also of various ultrashort laser pulses characteristics. A comprehensive review of such techniques can be found in Dorrer and Joffre [2001] to which the reader is referred for a detailed description of the many different possibilities demonstrated so far, and we will concentrate here on the methods that are most commonly applied, and those offering the most complete and detailed information on the pulse characteristics and therefore appearing as the most promising.

The first of them is second harmonic generation, which was proposed very early as a mean of measuring short pulses (Weber, Mathieu and Meyer [1966]). If obtained using two replicas of the pulse to be measured delayed by a time interval τ, it allows to deduce the

autocorrelation function of the pulse intensity with the measurement, for different delays of the quantity :

$$I_{SHG}(\tau) = \int_{-\infty}^{\infty} I(t)I(t-\tau)dt \qquad (1.33)$$

I representing the intensity profile of the pulse to be measured. Autocorrelators based on this technique (which can be exploited in two variants : the intensimetric mode, and the interferometric one, in which the autocorrelator is simply a Michelson interferometer associated with a frequency doubling crystal) are implanted on basically all subpicosecond laser systems. They allow to obtain not only the pulse duration (FWHM), but also some information on the pulse shape. They allowed for instance to realize that the pulse shape generated in femtosecond ti:sa oscillators were generally closer to the "squared-cosech" profile than to the exponential one described by eq. (1.11), the latter being still generally used due to its analytic simplicity. However, due to the symmetrical nature of the autocorrelation function, such a method is helpless in the case of asymmetrical pulses. It should also be mentioned that such methods are limited to measurements in the visible part of the spectrum essentially because the GVD of most non linear materials (which would produce an artificial lengthening of the pulse) is large in the UV range, thus limiting their thickness to values that preclude collection of a usable signal.

So, for the measurements of pulse durations in the UV or VUV range, one has to substitute to SHG another non-linear process allowing to couple the pulse to be measured to a well characterized optical pulse. Two photon absorption or ionization has often been employed to this aim. Note that the electronic nature of the non linear process is essential since it warrants – because of the fast response time of electrons – the accuracy of the measurement. For instance, the pulse duration of X-rays pulses generated by intense irradiation of a metallic target could be measured by monitoring the sidebands induced in the Auger electron spectrum of atomic Ar, subject to the combined irradiation the of X-ray pulse and a delayed IR subpicosecond pulse (Schins, Breger, Agostini, Constantinescu, Muller, Grillon, Antonetti and Mysyrowicz [1994]).

Needless to say, such methods are difficult to employ and generally do not give birth to apparatuses that could be considered as “measurement equipment”.

It is sometimes not enough to know the pulse duration. This was for instance the case in he example mentioned above of the measurement of the respective phases of the different high order harmonics. A commonly encountered example of such problem concerns the measurement of the so called “chirped” pulses, in which the frequency of light varies along the pulse. One then first has to locate the energy density in the time-frequency space, which is generally done using spectrographic techniques. One of them is based on the Frequency Resolved Optical Gating (FROG) principle (Kane and Trebino [1993]), consisting in measuring the spectrum of the pulse after gating through a correlation process. However, retrieval of the field, which requires the use of quite heavy algorithmic techniques, is a slow and uneasy task.

Interferometry-based techniques have emerged which appear to be the most powerful ones presently available. This is the case in particular of the Spectral-Phase Interferometry for Direct Electric field Reconstruction technique (SPIDER – Iaconis and Walmsley, [1998]) which is a frequency domain counterpart of shearing interferometry, allowing to obtain single-shot measurements of the spectral phase of ultrashort pulses (Dorrer, de Beauvoir, Le Blanc, Ranc, Rousseau, Rousseau and Chambaret [1999]). In this technique, whose experimental principle is sketched on Fig. 6, two time delayed frequency upshifted replica of the ultrashort pulse to be analyzed are generated by frequency mixing with a chirped pulse. In such a chirped pulse, the instantaneous frequency depends linearly on time ($\omega=t\alpha+\beta$), and will be supposed constant throughout the duration on the ultrashort pulse. If τ is the time delay between the two replicas, a frequency shear $\Omega=\tau\alpha$ is introduced between both replicas. One then measures the spectrum of the pair of upshifted replicas which consists in a series of fringes, whose structure is determined principally by the frequency shear Ω, but also bears information on the spectral phase of the original pulse as a continuous function of frequency (Fittinghof, Bowie, Sweetser, Jennings, Krumbugel, DeLong, Trebino and Walmsley [1996]; Lepetit, Cheriaux and Joffre [1995]). By

this technique it is thus possible, in a single laser shot, to obtain a complete information on both the amplitude and the phase of the EM pulse.

II. SPATIOTEMPORAL RESHAPING OF ULTRASHORT PULSES IN STATIONARY MEDIA.

The variety of applications of few-cycle optical pulses in different branches of physics is extending continuously. These applications range from time-domain spectroscopy of dielectrics (Smith, Auston and Nuss [1988]) to impulse photoionization of molecules, (Jones, You and Bucksbaum [1993]), new principles of imaging, suggested by Hu and Nuss [1995] and shape-dependent absorption of broadband pulses in the space plasma, examined by Akimoto [1996], to name just a few.

In any of such studies, one has to know the spatio-temporal parameters of the pulse at the target location. However, these parameters may change on the path between source and target. It was argued by Wolf [1986], [1987], that free-space propagation of a polychromatic radiation beam produces variations of the beam's spectrum, unless the radiation source possesses some particular coherence properties (which fortunately happens to be the case of many classical sources). Nevertheless, the general rule is that the spectrum does not have to be conserved upon propagation, and this particularly when broadband coherent radiation is considered. During the last two decades, great efforts were put into the understanding of the optics of broadband waveforms localized in time and space. Spatial and temporal dynamics of these waveforms cannot be analyzed separately, as in the quasimonochromatic case, but become coupled even in free space. The spatial frequencies, arising due to the finite transverse size of a real wave beam, provide free space dispersion, inducing changes in the pulse shape during propagation. The interplay of these effects in the dynamics of different waveforms, travelling both in dispersionless and dispersive media, is discussed below.

II.1 - Dynamics of ultrashort waveforms in dispersionless optical systems.

Propagation of ultrashort few-cycle pulsed beams in linear homogeneous lossless media is accompanied by a coupled evolution of their spatial and temporal parameters. To understand the fundamental role of the coupling between spatial and temporal reshaping of the pulse, it is worthwhile to show first how these processes are developing during propagation in free space (§ II.1.1), paragraph II.1.2 is devoted to spatial and temporal variations of waveforms passing through an optical system and waveform-preserving reflection on curvilinear mirrors is discussed in paragraph II.1.3.

II.1.1. : The interplay between transversal, longitudinal and temporal distortions of localized pulses is described by the paraxial equation for electric field $E(\mathbf{r}, z, t)$ (Einziger and Raz - 1987)

$$\Delta_{\perp} E = \frac{2}{c}\frac{\partial^2 E}{\partial z \partial t'} \tag{2.1.}$$

with $\Delta_{\perp} = \partial_x^2 + \partial_y^2$; $t' = t - zc^{-1}$. We will use a non-separable solution of eq. (2.1), which writes:

$$E(r,z,t) = \frac{iL_R}{q} F\left(t' - \frac{r^2}{2cq}\right) \tag{2.2}$$

here $r^2 = x^2 + y^2$, $q = z + iL_R$ and L_R is the diffraction length (Rayleigh range), F is an arbitrary function. The pulsed beam diffraction, arising due to its finite transversal size, induces, through the factor iL_R/q in eq. (2.2), propagation changes in the on-axis waveform. Presenting this factor in a form

$$\frac{iL_R}{q} = \frac{\exp(i\varphi)}{\sqrt{1 + \left(z/L_R\right)^2}} \quad ; \quad \varphi = Arctg\left(\frac{z}{L_R}\right) \tag{2.3}$$

one can link the factor $\left[1 + (z/L_R)^2\right]^{-1/2}$ with the pulse amplitude attenuation, meanwhile the phase φ is responsible for the evolution of the pulse shape : (2.2) is real at $z = 0$ to and purely imaginary for large z ($z >> L_R$). Parameter φ in (2.3) is known as the Gouy phase shift, and takes values from $-\pi/2$ to $\pi/2$. Independently of the choice of function F the coupling of its spatial and temporal variations comes from the complex space-dependent time shift $-r^2/2cq$. Its real part

$$t_S = -\frac{zr^2}{2c|q|^2} \tag{2.4}$$

is an actual time of arrival of the pulse at each plane. This shift is connected with the paraxial spherical phase front of radius

$$R(z) = \frac{|q|^2}{z} = z\left[1 + \left(\frac{L_R}{z}\right)^2\right] \tag{2.5}$$

The imaginary part of time shift $iL_R r^2/2c|q|$ determines the spatial distribution of pulse attenuation. Let us illustrate the spatio-temporal coupling phenomena, choosing the function F in a form (1.20), corresponding to the Poisson-spectrum pulse. The 1/e width of the real pulse F is

$$T = t_0\sqrt{\exp\left(\frac{2}{m}\right) - 1} \tag{2.6}$$

which can represent a large variety of pulses, the value m=1 relating to a single maximum of F, whereas large values of parameter m correspond to a growing number of oscillations with almost constant frequency $\omega_m = mt_0^{-1}$ in the central part of the pulse. To examine the forming of a spatiotemporal structure in the course of paraxial propagation of the pulse (2.2) one can use eq. (1.20), replacing the time t' by a complex time $t' - r^2/2cq$ and multiplying the function F (1.20) by the Gouy factor

$$E(r,z,t) = \frac{iL_R}{q}\left(\frac{it_0}{t' - \frac{r^2}{2cq} + it_0}\right)^m \tag{2.7}$$

Using the definition of q, and with the help of (2.5), one can rewrite eq. (2.7) in a form

$$E(r,z,t) = \frac{iL_R}{q}\left(\frac{t_0}{t_0 + \frac{r^2 L_R}{2c|q|^2}}\right)^m \left[\frac{i\left(t_0 + \frac{r^2 L_R}{2c|q|^2}\right)}{\left(t' - \frac{r^2}{2cR}\right) + i\left(t_0 + \frac{r^2 L_R}{2c|q|^2}\right)}\right]^m \tag{2.8}$$

of which, according to (1.20), one should take the real part. One can see that solution (2.8) derives from (2.7) through a time shift, connected with the spherical pulse fronts of radius R (2.5) and replacement of parameter t_0 by $t_0 + r^2 L_R \big/ 2c|q|^2$. These changes result in an increase of the pulse duration T, as compared with (2.6)

$$T = t_0 \left(1 + \frac{r^2 L_R}{2ct_0 |q|^2} \right) \sqrt{\exp\left(\frac{2}{m} \right) - 1} \tag{2.9}$$

The frequency of oscillations being redshifted :

$$\omega_m = m \left(t_0 + \frac{r^2 L_R}{2c|q|^2} \right)^{-1} \tag{2.10}$$

As shown by Porras [1999], the off-axis spatial structure of the pulse (2.8) is characterized by the factor $\left(1 + r^2 L_R \big/ 2ct_0 |q|^2\right)^{-m}$, indicating a decrease of the pulse amplitude when moving away from the axis. The Gouy factor iL_R/q describes the pulse temporal reshaping, including its polarity reversal during the pulse travel from $z << -L_R$ to $z >> L_R$ (Fig. 7).

It should be pointed out that the pulse spectrum has an essential influence on the dynamics of its spatio-temporal evolution. The above mentioned results relate to the Poisson-spectrum pulses (1. 21). This spectrum, determined by two parameters only - m and t_0 - proves to be flexible enough for modeling of such phenomena as pulse lengthening, frequency redshifting and polarity reversal. Such transformations were observed experimentally by Feng and Winful [1998] in the diffraction of ultrashort pulses.

The above analysis was treating the pulse propagation in an homogeneous medium. We now turn to the study of the effects arising from transportation of such pulses through an optical system.

II.1.2. Let us consider the spatio-temporal transformation of an ultrashort pulse with Poisson spectrum (1.21), passing through a thin lens. The main features of such a transformation can be revealed in a simple case, that of the so-called isodiffracting pulses. These pulses, characterized by a frequency-independent Rayleigh range, were examined by Melamed and Felsen [1998].

Feng, Winful and Hellwarth [1999] showed that such pulses can be generated, e.g., in a cavity resonator consisting of two curved mirrors of equal radii of curvature R, separated by a distance L. The confocal parameter for this geometry is given by

$$d = \frac{2\pi W^2}{\lambda} = \sqrt{L(2R-L)} \tag{2.11}$$

Here W is the beam waist, $W \approx \sqrt{\lambda}$, and the Rayleigh range is

$$L_R = \frac{1}{2}\sqrt{L(2R-L)} \tag{2.12}$$

This fixed confocal parameter provides the same values of wave front radius of curvature $R(z)$ for all the wavelengths and thus for the entire pulse.

Making a one-sided inverse FT of the isodiffracting pulse with Poisson-spectrum (1. 21) with m=3, Feng and Winful [1999] obtained the following expression for the field :

$$E = \frac{iA_0}{q}\frac{\exp[-3iArctg(T)]}{(1+T^2)^{3/2}\left[1+\dfrac{r^2}{a^2(z)}\right]^3} \tag{2.13}$$

where parameter $q = z + iL_R$ represents the Gouy phase shift and the z-dependent amplitude attenuation factor; the normalized local time scale T is

$$T = \frac{t - \dfrac{1}{c}\left[z + \dfrac{r^2}{2R(z)}\right]}{t_0\left[1+\dfrac{r^2}{a^2(z)}\right]} \tag{2.14}$$

Here the radius of curvature $R(z)$ is defined in (2.5), the beam width $a(z)$ is given by

$$a^2(z) = 2ct_0 L_R\left[1+\left(\frac{z}{L_R}\right)^2\right] \tag{2.15}$$

The q parameter of the pulse is linked to the values of $R(z)$ and $a(z)$ by

$$\frac{1}{q} = \frac{1}{R(z)} - \frac{2ict_0}{a^2(z)} \tag{2.16}$$

Let us consider such a pulse, passing through a thin non-dispersive lens with focal length f, placed in the vacuum at plane z=0. Upon propagation through this lens the entire pulse can be characterized by a new value of parameter $q=q_2$, which is related to the parameter q_1 of incoming pulse by the so-called ABCD transformation, developed by Dijaili, Dienes and Smith [1990]

$$q_2 = \frac{Aq_1 + B}{Cq_1 + D} \tag{2.17}$$

Here $q_1=d_1+iL_R$, d_1 being the distance from the beam waist of the incoming pulse to the lens. For the pulse passing through the aforesaid thin lens to any point z_2, the values A,B,C and D were found by Feng and Winful [1999]:

$$A = 1 - \frac{z_2}{f} \quad ; \quad B = z_2 \quad ; \quad C = -1/f \quad ; \quad D = 1 \tag{2.18}$$

(2.18), (2.17) and (2.16) give the transformed q parameter at z_2

$$q_2 = \frac{\left(1 - z_2 f^{-1}\right)\left(d_1 + iL_R\right) + z_2}{1 - \left(d_1 + iL_R\right) f^{-1}} \tag{2.19}$$

Making use of (2.16) with the value $q=q_2$ (2.19) yields the values of the new Rayleigh range L'_R and new beam waist $a^2(d_2)$, located at the distance d_2 from the lens :

$$L_R^{'} = \frac{L_R}{K} \quad ; \quad a^2\left(d_2\right) = \frac{2ct_0}{K} \tag{2.20}$$

$$d_2 = \frac{1}{K}\left[d_1 - f^{-1}\left(d_1^2 + L_R^2\right)\right] \quad ; \quad K = \left(1 - d_1 f^{-1}\right)^2 + \left(L_R f^{-1}\right)^2 \tag{2.21}$$

The total phase shift between the input and output beam waist is

$$\varphi = Arctg\frac{L_R}{f - d_1} \tag{2.22}$$

These results illustrate the spatiotemporal evolution of pulse (2.14), caused by its passage through a thin dispersionless lens in vacuum. The following salient features of such evolution can be stressed out

(i) The phase shift, introduced by the lens, can change drastically the pulse's temporal profile at the focus. For instance in a case $d_1=f$, it follows from eq. (2.22), that $\varphi=\pi/2$; herein a unipolar (bipolar) pulse is transformed into a bipolar (unipolar) one.

(ii) Considering the planes $z=d_1$ and $z=d_2$ as the object and image planes with respect to the beam waists, one can see that the image pulses are different both is space (beam size) and in time (pulse width) at different locations

(iii) The variations of the spatial and temporal structures of the off-axis field at the beam waist ($z=d_2$) can be found by means of substitution of parameters (2.20)-(2.21) into the expression (2.14), meanwhile the on-axis pulse width remains invariant.

Feng and Winful [1999] showed that the spatio-temporal reshaping of Poisson-spectrum pulses, reflected from a concave spherical mirror with radius R, is described by formulae (2.19)-(2.22) after replacement of the lens focal length f by the mirror radius R. Another geometry of curvilinear mirror providing invariance of the reflected pulse shape, is considered now.

II.1.3. To design curvilinear reflectors, with the purpose of controling the properties of transient fields, Bateman [1955] developed an elegant time-domain approach to the analysis of EM field in a free space. Following this approach, let us introduce a vector $\mathbf{M}$, which is the linear combination of electric ($\mathbf{E}$) and magnetic ($\mathbf{H}$) components of this field (assumed to be linearly polarized):

$$\mathbf{M} = \mathbf{E} + \mathrm{i}\,\mathbf{H} \tag{2.23}$$

The equation governing vector **M**, can be derived from the Maxwell equations

$$\nabla \times \mathbf{M} = -\frac{i}{c}\frac{\partial \mathbf{M}}{\partial t} \tag{2.24}$$

Further, representing vector **M** by scalar fields U and ψ in the form

$$\mathbf{M} = \nabla U \times \nabla \psi \tag{2.25}$$

and substituting eq (2.25) into eq (2.24), we obtain an equation, describing these scalar fields:

$$\nabla U \times \nabla \psi = -\frac{i}{c}\left(\frac{\partial U}{\partial t}\nabla \psi - \frac{\partial \psi}{\partial t}\nabla U\right) \tag{2.26}$$

It should be noted that, as well as vector **M**, defined by eq (2.25), any other vector $\mathbf{M_1}$

$$\mathbf{M}_1 = F(U,\psi)\nabla U \times \nabla \psi \tag{2.27}$$

containing any arbitrary function $F(U,\psi)$ also obeys eqn (2.24). The determination of vector **M** for the scattered field is appreciably easier than the traditional solution of the scattering problem. The components of this vector being known, the separation of their real and imaginary parts yields the fields **E** and **H** (2.24).

This notation proves to be important for the analysis of some scattered pulsed fields. A linearly polarized plane wave with the components E_x and H_y , travelling in the z-direction, may be described by means of scalar functions

$$U_1 = x + iy \quad ; \quad \psi_1 = z + ct \tag{2.28}$$

Substitution of eq. (2.28) into eq. (2.25) yields $M_x=i$, $M_y=-1$; comparing this result with the definition (2.24), we obtain the dimensionless values of the components of this plane wave : $E_x=1$, $H_y=-1$. An arbitrary waveform of this field may be written, according to eq. (2.27), as

$$\mathbf{M}_1 = F_1(\psi_1)\nabla U_1 \times \nabla \psi_1 \tag{2.29}$$

Proceeding in a similar fashion, one can find the representation of a diverging spherical wave, using the coordinates ρ, θ, ψ. Introducing the scalar functions

$$U_2 = e^{-i\varphi} tg\left(\frac{\theta}{2}\right) \quad ; \quad \psi_2 = \rho - ct \tag{2.30}$$

one can find the components of vector $\mathbf{M_2}$ for this field:

$$M_{2\rho} = 0 \quad ; \quad M_{2\theta} = -\frac{ie^{-i\varphi}}{\rho(1+\cos\theta)} \quad ; \quad M_{2\varphi} = -iM_{2\theta} \tag{2.31}$$

By analogy with eq (2.29), vector $\mathbf{M}_2$ can be presented in a form containing an arbitrary scalar function

$$\mathbf{M}_2 = F_2(\psi_2)\nabla U_2 \times \nabla \psi_2 \tag{2.32}$$

We can now examine the scattering of an incident plane wave $\mathbf{M}_2$ on some curvilinear surface R. Since eq (2.24), governing the vector $\mathbf{M}_2$, is linear, the linear combination

$$\mathbf{M}_2 = F_1(\psi_1)\nabla U_1 \times \nabla \psi_1 + KF_2(\psi_2)\nabla U_2 \times \nabla \psi_2 \tag{2.33}$$

representing the total field of the incident and scattered wave, must also be a solution of this equation; the constant K in (2.33) has to be defined from the boundary conditions at the scattering surface R.

Let us consider, using this approach, the scattering of an arbitrarily shaped waveform with a plane wave front, incidenting on the convex side of a perfectly conducting axisymmetrical surface R along its axis of symmetry z (Fig. 8). Assuming this wave to be linearly polarized, one can rewrite the scalar functions U_1 and ψ_1 (2.28) in spherical coordinates:

$$U_1 = \rho \sin\theta e^{i\varphi} \quad ; \quad \psi_1 = -\rho\cos\theta + ct \tag{2.34}$$

and substituting eq (2.34) to eq (2.33), we can find vector $\mathbf{M}$:

$$M_\rho = F_1 \sin\theta e^{i\varphi} \tag{2.35}$$

$$M_\theta = F_1 \cos\theta e^{i\varphi} + \frac{KF_2 e^{-i\varphi}}{\rho(1+\cos\theta)} \tag{2.36}$$

$$M_\varphi = iF_1 e^{i\varphi} - \frac{KF_2 e^{-i\varphi}}{\rho(1+\cos\theta)} \tag{2.37}$$

It is of interest to examine the case of an arbitrary waveform which remains invariant in the course of scattering, i.e. $F_1=F_2=F$. Since the surface R is supposed to be perfectly conducting, the tangential component of the electric field $E_\varphi = ImM_\varphi$ should vanish on this surface, which determines the value of the constant K:

$$K = \rho_0(1+\cos\theta) \tag{2.38}$$

Here ρ_0 and θ are the polar coordinates of the curve forming the axisymmetric surface by rotation around the z axis. Curve (2.38) is a parabola; its pole is located at the center of the coordinate system (Fig. 8). Hence the surface R is a paraboloid. The components of the EM field, scattered by this paraboloid, are determined directly from eq (2.36)-(2.37)

$$H_\theta = -E_\varphi = \frac{\rho_0}{\rho}\cos\varphi F(\rho - ct)$$
$$H_\varphi = E_\theta = -\frac{\rho_0}{\rho}\sin\varphi F(\rho - ct) \qquad (2.39)$$
$$E_\rho = H_\rho = 0$$

Using these fields, one can write the radial component of the energy flow, carried by scattered waveform, as

$$P_\rho = \frac{c}{4\pi}\left(\frac{\rho_0}{\rho}\right)^2 F^2(\rho - ct) \qquad (2.40)$$

Thus we have obtained the time-domain description of the scattered wave. The main features of this reflector are : (i) the Pointing vector of the scattered field is directed radially: $P_\rho \neq 0; P_\varphi = P_\rho = 0$; (ii) this result is valid for an arbitrary waveform; (iii) the preservation of the scattered waveform is probably a unique property of a paraboloid reflector.

This example shows the possibilities of elegant time-domain method developed by Bateman [1955] for the problem of diffraction and scattering of transients, treated traditionally by computer simulations. It is worth noticing that, more than forty years later, the use of parabolic mirrors is considered as the only way of focusing efficiently (i.e. without lengthening the pulse) ultrashort laser pulses.

II.2. Evolution of transients in dispersive media .

The traditional analysis of wave dispersion phenomena is based upon the supposition of a slow accumulation of pulse envelope distortions in the course of propagation in dispersive media. The characteristic length for such an accumulation $L_d = 2t_0 / |K_{\omega\omega}| -$ depends upon the second-order dispersion of the medium, described by the factor $K_{\omega\omega} = \partial^2 k / \partial\omega^2$, where $k=k(\omega)$ is the dispersion relation. Some types of pulse distortions typical, in particular, of fiber optics, are determined by means of third order dispersion; the analysis of these effects was given by

Agrawal [1994]. A forthcoming improvement of this approach, taking into account the fourth order dispersion, was considered by Karlsson and Hook [1994]. Brabec and Krausz [1997] derived the generalized equation, describing the influence of an arbitrary order dispersion on the evolution of a pulse envelope.

Alternatively, the effect of non-stationary propagation of ultrashort one or few cycle waveforms in dispersive media can be investigated by means of the temporal variations of electric strength itself. This approach is presented in this chapter : simple analytical expressions for time-dependent electric strength of a flexible waveform in a medium with second-order dispersion are given in paragraph II.2.1. paragraphs II.2.2 and II.2.3 show the rapid deformation of transient electric and magnetic components in plasma-like media and waveguides by means of exact time-domain non-sinusoidal solutions of Maxwell equations without using the concept of dispersion.

II.2.1. Let us consider first the spatiotemporal evolution of localized waveform in a lossless medium with an arbitrary dispersion $\omega=\omega(k)$. Following Nodland [1997], one can use the flexible presentation of an initial waveform as a superposition of spatially modulated Gaussian waveforms

$$E_0(z)=\sum_{m=1}^{n} f_m \exp\left(-a_m z^2\right)\cos(b_m z) \tag{2.41}$$

Here f_m, a_m and b_m are some real constants, and $a_m>0$. The FT of (2.41) can be written as

$$A(k)=\frac{1}{2\pi}\int_{-\infty}^{\infty} E_0(z)\exp(-ikz)dz=\frac{1}{4\pi}\sum_{m=1}^{n}\frac{f_m}{\sqrt{a_m}}\left\{\exp\left[-\frac{(k-b_m)^2}{4a_m}\right]+\exp\left[-\frac{(k+b_m)^2}{4a_m}\right]\right\} \tag{2.42}$$

The dominant wavenumbers in eq. (2.42) are $k=\pm b_m$; expanding the dispersive relation up to second order around each point $\pm b_m$, we obtain

$$\omega(k\pm b_m)=s_0(\pm b_m)+ks_1(\pm b_m)+k^2 s_2(\pm b_m) \tag{2.43}$$

the coefficients s_1 and s_2 depend upon the derivatives $\partial\omega/\partial k$ and $\partial^2\omega/\partial k^2$. Since the expression $A(k)$ (2.42) is real, one can present the electric field $E(z,t)$ in a form

$$E(z,t)=\int_{-\infty}^{\infty}A(k)\cos[kz-t\omega(k)]dk \tag{2.44}$$

Substitution of (2.42) and (2.43) into (2.44) brings the expression for electric field as a sum of $2n$ terms, all of them centered on the major wave numbers $\pm b_m$ with $1\le m\le n$

$$E(z,t)=\frac{1}{4\sqrt{\pi}}\sum_{m=1}^{n}\frac{f_m}{\sqrt{a_m}}\int_{-\infty}^{\infty}dk\exp\left[-\frac{(k-b_m)^2}{4a_m}\right]\cos\left\{-ts_0(b_m)+k[z-ts_1(b_m)]-k^2ts_2(b_m)+\langle b_m\to -b_m\rangle\right\} \tag{2.45}$$

The integral in (2.45) can be performed analytically, yielding:

$$E(z,t)=\frac{1}{4\sqrt{\pi}}\sum_{m=1}^{n}\frac{f_m}{\sqrt{a_m}}\left\{\sqrt[4]{f_m}\exp\left[\frac{F_m}{4a_m}A_m\cos(B_m)\right]-\frac{1}{2}Arctg[4ta_ms_2(b_m)]+\langle b_m\to -b_m\rangle\right\} \tag{2.46}$$

with

$$A_m=tb_ms_2(b_m)[z-ts_1(b_m)]-\frac{1}{4}[z-ts_1(b_m)]^2-t^2b_m^2s_2^2(b_m) \tag{2.47}$$

$$B_m=F_m\left\{\frac{b_m[z-ts_1(b_m)]-t[s_0(b_m)+b_m^2s_2(b_m)]}{16a_m^2}+\frac{1}{4}ts_2(b_m)[z-ts_1(b_m)]-t^3s_0(b_m)s_2^2(b_m)\right\} \tag{2.48}$$

$$F_m=\left[(4a_m)^{-2}+t^2s_2^2(b_m)\right]^{-1} \tag{2.49}$$

Considering each mth pair in presentation (2.46), one observes that the amplitude of this mth pair, maximal at the points $\pm b_m$, decays exponentially when one moves away from these points; the amplitudes are 1/e of their maximal value when k is at the distance $\pm 2\sqrt{a_m}$ from the point $\pm b_m$.

Thus, each pair makes a significant contribution to the field only in two areas of the $\omega(k)$ line. The advantages of this approximate description can be summarized as : (i) the dispersion law is arbitrary, (ii) the presentation of an initial waveform is flexible, each sinusoidal wave packet in (2.41) is characterized by three free parameters, (iii) the localized field is presented as a sum of elementary functions. At the same time one has to mention some shortcomings of this approach : (i) An initial waveform $E(z)$ (2.41) is supposed to be known inside the medium. This supposition seems to be justified when considering a waveform near a source located inside the medium. But this waveform remains to be found when the pulse has to travel a large distance $z>>\omega_k t$ from the

source; (ii) Presentations (2.41) are restricted to symmetrical waveforms only, (iii) The result (2.46) is restricted to the second-order dispersion and it is not easy to generalize this result, including, e.g., the third-order dispersion.

Considering this, it is worthwhile to discuss another statement of the pulse dynamics problem, considering the pulses generated by a source, located outside the dispersive medium. Using the continuity conditions for EM fields on the interface of this medium, we will find the non-stationary waveforms inside the medium. Herein the impulse reflection and refraction problems have to be solved simultaneously. It is shown below how exact non-stationary time domain solutions of Maxwell equations can describe the waveforms dynamics without any suppositions about smallness or slowness of dispersive distortions of fields in the medium; thus, in particular, the expansions (2.43) are not needed in this approach.

II.2.2. Realistic models of ultrashort EM transients, generated by existing optical systems, often differ from idealized cos-Gaussian waveforms. They can present uneven distances between zero-crossing points and asymmetric waveforms, including a well-defined leading front and slowly damping tail, and can be, as well as the reflected ones, represented in the time range 0 to ∞ by linear superposition of Laguerre functions L_n (1.18); the same superposition for the reflected pulses can be written replacing coefficients a_n in (1.17) by b_n . Since both electric and magnetic components of these pulses are equal to zero at the pulse's front edge and $L_n(0) = 1$(Fig. 2), the coefficients a_n and b_n have to obey conditions

$$\sum_{n=0}^{\infty} a_n = 0 \quad ; \quad \sum_{n=0}^{\infty} b_n = 0 \tag{2.50}$$

The coefficients a_n, characterizing the incident pulse, are supposed to be known, the coefficients b_n have to be found simultaneously with the coefficients d_q defining the field components in the plasma-like medium (eq. 1.44).

For simplicity let us consider the normal incidence of Laguerre waveforms from vacuum on the half-space $\eta \geq 0$, filled by a plasma. To use the continuity conditions for incident E_i, H_i, reflected E_r, H_r and transmitted E_t, H_t fields on a plane $\eta = 0$

$$E_i + E_r = E_t \quad ; \quad H_i + H_r = H_t \tag{2.51}$$

Presenting the incident and reflected waveforms on a plane $\eta = 0$ by means of Laguerre functions (1.18) and transmitted fields by means of non-separable solutions of Maxwell equations (1.44), one can rewrite the continuity conditions (2.51) in a form

$$\sum_{n=0}^{\infty}(a_n + b_n)L_n(t) = -\frac{A_0\Omega}{c}\sum_{q_0}^{\infty} d_q e_q(\tau) \tag{2.52}$$

$$\sum_{n=0}^{\infty}(a_n - b_n)L_n(t) = -\frac{A_0\Omega}{c}\sum_{q_0}^{\infty} d_q h_q(\tau) \tag{2.53}$$

Multiplying equations (2.53)-(2.53) by the Laguerre functions $L_n(t)$, integrating both sides of these equations with respect to t and using the orthonormality of Laguerre functions (1.19) we obtain an infinite set of equations:

$$a_n + b_n = -\frac{A_0\Omega}{c}T_{1n}(\alpha) \tag{2.54}$$

$$a_n - b_n = -\frac{A_0\Omega}{c}T_{2n}(\alpha) \tag{2.55}$$

where $\alpha = \Omega t_0$, and

$$T_{1n} = \sum_{q_0}^{\infty} d_q P_{nq}(\alpha) \quad ; \quad T_{2n} = \sum_{q_0}^{\infty} d_q Q_{nq}(\alpha) \tag{2.56}$$

$$P_{nq}(\alpha) = \int_0^{\infty} dx L_n(x) e_q(\alpha x) \quad ; \quad Q_{nq}(\alpha) = \int_0^{\infty} dx L_n(x) h_q(\alpha x) \tag{2.57}$$

The dimensionless quantities P_{nq} and Q_{nq} can be considered as matrix elements, describing the excitement of q-th harmonic of non-sinusoidal field by n-th Laguerre waveform.

The systems (2.54)-(2.57) allow the simultaneous calculation of coefficients b_n and d_q, characterizing the reflected and transmitted EM fields. Let us outline some properties of this system:

(i). The coefficients P_{nq} and Q_{nq} (2.57) depend only upon the parameter α ,which may be considered as the ratio of two characteristic times - pulse duration t_0 and plasma period Ω^{-1}.

There are no restrictions for the values of t_0 and Ω in the model discussed here. Thus, speaking about the propagation of "ultrashort" pulse in plasma – like media, one has to keep in mind that the same pulse can be considered as long or short not depending on the absolute value of its duration, but on the comparison of this value with the dispersive time-scale of the medium of propagation.

(ii). Due to the non-stationary regime of pulse reflection, the reflected transient can contain some Laguerre waveforms which are absent in the incident pulse. It means that in the relevant pair of equations (2.52)-(2.53) for n-th Laguerre waveform one has a_n=0, but $b_n \neq 0$. e.g., considering an incident waveform of the type $F_1(x)=L_0(x)-L_1(x)$ (a_0=1, a_1=-1), the reflected pulse contains, along with transients L_0 and L_1, the series of transients L_2 to L_7 with significant amplitudes although a_2 to a_7 are all equal to zero. Generation of these transients, providing reshaping of the reflected signal (Fig. 9 a), can be viewed as a result of shock excitement of the dispersive medium by the ultrashort waveform.

Solving system (2.54)-(2.55), we will find n coefficients b_n for the reflected pulse and n coefficients d_q for the refracted field. All these coefficients are real. Substituting the coefficients to eq. (1.44), we can present both electric and magnetic components of the EM field inside the medium.

It is noticeable that coefficients b_n describing the reflected Laguerre waveform L_0, can be expressed without solving the whole system (2.54)-(.2.55). Doing this, Shvartsburg [1999] showed that the reflection coefficient of Laguerre waveform L_0 can be expressed simply as a function of coefficient α only :

$$R_0 = \frac{b_0}{a_0} = -(\alpha D)^2 = -\frac{4\alpha^2}{\left(1+\sqrt{1+4\alpha^2}\right)^2} \qquad (2.58)$$

The graph $R_0(\alpha)$ is shown on Fig. 9b. As could be expected, in the case of a rarefied plasma ($\alpha \to 0$) the coefficient R_0 is small ($R_0=-\alpha^2$) and proportional to plasma density; in the opposite case ($\alpha >> 1$, dense plasma) the reflection is almost total ($R_0 \to -1$) .

II.2.3. The appearance of optoelectronic sources and receivers of subpicosecond pulses of terahertz (THz) EM radiation has generated much interest into the quasi-optical methods of spatiotemporal shaping of these pulses. Many methods, used in the microwave domain, were scaled down to the THz domain. A continuous refinement of THz generation techniques during the last decade has made several important applications possible, including time-domain far IR spectroscopy (Keiding, [1994]), THz imaging (Hu and Nuss, [1995]) and generation of tunable narrow-band THz radiation (Weling, Hu, Froberg and Auston, [1994]). These applications require a specific pulse form, such as, e.g., the half-cycle pulses such as the ones mentioned in chapter I-2. Rapid spatiotemporal shaping of almost half-cycle THz radiation, based on diffraction of waves on conductive aperture with finite thickness, was observed by Bromage, Radic, Agrawal, Stroud, Fauchet and Sobolewski [1998].

An effective method of THz pulses shaping, based on dispersive passage through a segment of metallic waveguide, was demonstrated by Mc Gowan, Gallot and Grischkowsky [1999]. In their experiment the pulses were coupled into the circular metal waveguide through a silicon lens and coupled out with a second silicon lens. The ~1 ps input pulse was stretched to 70 ps while propagation through the waveguide segment, equal to 80 initial pulse spatial lengths. The waveguide propagation is characterized by a multimode behavior and late time oscillations; the typical envelope of these oscillations in the outcoming pulse based on the measurements made by Mc Gowan, Gallot and Grischkowsky [1999], is shown on Fig. 10.

It is noticeable that a similar waveform can be obtained by means of direct time domain solutions of Maxwell equations for hollow circular waveguide with perfectly conducting walls. Let us consider the simplest axisymmetrical vortical TE_{01} mode in this waveguide, with E_φ, H_ρ and H_z components. The component E_φ is known to obey the wave equation

$$\frac{\partial^2 E_\varphi}{\partial \rho^2}+\frac{1}{\rho}\frac{\partial E_\varphi}{\partial \rho}-\frac{E_\varphi}{\rho^2}+\frac{\partial^2 E_\varphi}{\partial z^2}-\frac{1}{c^2}\frac{\partial^2 E_\varphi}{\partial t^2}=0 \qquad (2.59)$$

Setting E_φ in a form:

$$E_\varphi = F(\rho) f(z,t) \tag{2.60}$$

and substituting (2.60) into (2.59), one obtains the factorized equations, governing the functions F and f

$$\frac{\partial^2 F}{\partial \rho^2} + \frac{1}{\rho}\frac{\partial F}{\partial \rho} + k_\perp^2 F = 0 \tag{2.61}$$

$$\frac{\partial^2 f}{\partial z^2} - \frac{1}{c^2}\frac{\partial^2 f}{\partial t^2} = k_\perp^2 f = 0 \tag{2.62}$$

Solutions of eq. (2.61), restricted to positive values of the "separation constant" $k_\perp^2$ are given by the Bessel function

$$F = J_1(k_\perp \rho) \tag{2.63}$$

The values of constant $k_\perp$, determined from boundary condition $E_\varphi=0$ on the waveguide inner surface, are discrete

$$k_{\perp n} = \frac{x_n}{R} \quad , \quad n = 1,2,3,.... \tag{2.64}$$

where x_n are the roots of equation $J_1(x_n)=0$. The smallest value of x_n is known to be $x_1=3.84$. Considering eq. (2.64) and introducing the normalized variables $\tau_n = ctk_{\perp n}$ and $\eta_n = zk_{\perp n}$ one can rewrite eq. (2.62) in the form of Klein-Gordon equation (1.37). Substitution of solutions of this equation, expressed via the non-separable harmonics (1.44)-(1.45), and solutions F (2.63) into formula (2.60) yields the presentation of electric strength E_φ in a time domain

$$E_\varphi = \frac{A_0}{4}\sum_{n=1}^{\infty} J_1(k_{\perp n}\rho)\sum_{q=3}^{\infty} d_{nq}\left[\psi_{q-2}(\tau_n,\eta_n) - 2\psi_q(\tau_n,\eta_n) + \psi_{q+2}(\tau_n,\eta_n)\right] \tag{2.65}$$

The field components H_ρ and H_z can be found from Maxwell equations

$$H_\rho = -\frac{A_0}{4}\sum_{n=1}^{\infty} J_1(k_{\perp n}\rho)\sum_{q=3}^{\infty} d_{nq}\left[\psi_{q-2}(\tau_n,\eta_n) - \psi_{q+2}(\tau_n,\eta_n)\right] \tag{2.66}$$

$$H_z = -\frac{A_0}{2}\sum_{n=1}^{\infty} J_0(k_{\perp n}\rho)\sum_{q=3}^{\infty} d_{nq}\left[\psi_{q-1}(\tau_n,\eta_n) - \psi_{q+1}(\tau_n,\eta_n)\right] \tag{2.67}$$

These solutions, which are both non-stationary and non-sinusoidal, differ totally from the traditional presentation of monochromatic cw train in the same axisymmetrical modes in frequency domain

$$E_\varphi = \sum_{n=1}^{\infty} J_1(k_{\perp n}\rho)\exp[i(\beta_n z - \omega t)]$$

$$H_\rho = -\frac{c}{\omega}\sum_{n=1}^{\infty} A_n \beta_n J_1(k_{\perp n}\rho)\exp[i(\beta_n z - \omega t)] \quad ; \quad \beta_n = \sqrt{\frac{\omega^2}{c^2} - k_{\perp n}^2} \tag{2.68}$$

$$H_z = -\frac{ic}{\omega}\sum_{n=1}^{\infty} A_n k_{\perp n} J_0(k_{\perp n}\rho)\exp[i(\beta_n z - \omega t)]$$

The excitation efficiency of the modes in a waveguide by an external source depends upon the geometry of the problem, spatial scales and polarization structure of the exciting pulse. To evaluate the excited modes in the circular waveguide one has to perform a numerical overlap integral between the incoming field and the field of the individual mode over the waveguide cross-section. After this one can calculate the reflected field and the field, launched into the waveguide, by means of the time-domain sets of equations (2.54)-(2.55), written for each mode. Usually, the main contributions to these fields originate from a few modes only.

The spatiotemporal structures of non-separable harmonics in (2.65)-(2.68) are qualitatively similar. The whole pulse envelope contains the weighted sum (2.65) of such harmonics. Moreover, the asymptotics of Bessel functions $J_1(u_n)$; $u_n = \sqrt{\tau_n^2 - \eta_n^2}$ for $u_n >> 1$ yields the late time asymptotics of harmonics e_q in the form of damping sinusoids; e.g.;

$$e_3(\tau_n, \eta_n) = \sqrt{\frac{2}{\pi u_n}}\sin\left(u_n - \frac{3\pi}{4}\right) \tag{2.69}$$

The frequencies of these sinusoids are given by the modes cut-off frequencies (2.64) $\Omega_n = x_n c R^{-1}$. Thus, the tail of the pulse will contain the waveguide's eigenfrequencies. This "ringing" with a periods of about 1 ps, was observed by Mc Gowan, Gallot and Grischkowsky [1999] in a pulse passed through a circular waveguide. Another manifestation of the same effect – "ringing" of reflected radiation – is considered in paragraph II.3.

II-3. Broadband reflectivity in transient optics.

Electromagnetic fields of solitary ultrashort waveforms, reflected from targets, possess some characteristics distinguishing them from cw trains reflected from the same targets. The response of a target contains often some useful information about the nature of reflection. The discovery of reliable sources of picosecond single-cycle waveforms and femtosecond laser pulses has opened a new field of research, connected with the pulsed excitement of EM eigenoscillations in resonant media by some spectral components of the incident wideband pulse. The re-emission of the excited eigenfrequencies can stimulate a dramatic reshaping of the reflected pulse and formation of a long ringing tail of this pulse. The shorter the pulse and the wider its spectral bandwidth, the more likely such resonant effect will arise. The physical fundamentals of identification of complex targets due to their ringing in the microwave range, presented by Baum, Rothwell, Chen and Nyquist [1991], stimulated the development of the similar concepts in impulse optics. Such a ringing is a general wave pulse effect, usual to the different scatterers and spectral ranges. For instance, the scattering of broadband IR pulses on a metallic surface containing microtips, can lead to excitement of IR eigenmodes in these microtips, and to reshaping of the scattered waveforms. A method of fast non-destroying control of surface mechanical imperfections, based on these resonant deformations of scattered pulses, was suggested by Maradudin [1999]. Examples of resonant ringing of continuous dispersive media are discussed in paragraph II.3.1.

On the contrary, the non-resonant phenomena in broadband reflectivity of frequency-selective plane interface of a thin heterogeneous film are considered in the paragraph II.3.2. Strong inhomogeneity –induced dispersion of such a film provides drastic distortions of both the reflected and transmitted waveforms. Generalization of Fresnel's reflectivity laws, taking into account the geometric dispersion, habitual to curvilinear reflecting interfaces of transparent dielectrics, is illustrated in the paragraph II.3.3.

II.3.1. Reflection spectra of crystals reveal pronounced structures nearby the material resonances. The reflection should show a transient behavior in the case of pulsed excitement as a consequence of the frequency dependence of the reflection coefficient $R(\omega)$. The reflected pulse $E_r(t)$ is related to the initial pulse spectrum $E_i(\omega)$ through the Fourier integral:

$$E_r(t) = \int_{-\infty}^{\infty} R(\omega) E_i(\omega) d\omega \tag{2.70}$$

To consider the possibilities of transient reflection one can use the model of non-local medium, where the dielectric function depends upon the wave vector k

$$\varepsilon(\omega) = \varepsilon_S + \frac{4\pi\beta\omega_0^2}{\omega_0^2 - \omega^2 - i\omega\Gamma + \frac{\hbar\omega_0}{M}k^2} \tag{2.71}$$

Here ω_0 and Γ are the eigenfrequency and damping constant of the oscillator, β is the polarizability, ε_S is the background dielectric constant, M is an effective exciton/polariton mass. In a limiting case $M \to \infty$, the dielectric function $\varepsilon(\omega)$ (2.71) describes a Lorentz resonant medium. The non-zero spectral bandwidth of the incident pulse and the dispersion of reflection coefficient $R(\omega)$ result in the reshaping of the reflected waveform. This approach was shown by Agrawal, Birman, Pattanayak and Puri [1982] to be suitable for the interpretation of different types of transients, formed by interaction of picosecond pulses in the infrared range with GaAs and CdS crystals near the excitonic resonances.

To illustrate the temporal reshaping of the reflected pulses, induced by excitonic resonances, Aaviksoo and Kuhl [1989] used the reflection of P-polarized pulses from the medium (2.71) close to the Brewster angle γ_B. They showed that the general shape of the reflected pulse is divided into a fast non-resonant contribution, which is due to the background dielectric constant and gives rise to a quasi-steady-state reflection of the incident pulse; it vanishes at Brewster angle, allowing to reveal the resonant contribution to reflection, which is responsible for the delayed tail (Fig. 11). One can see that the duration of the ringing tail excited

by the pulse, may be much longer than the characteristic pulse halfwidth. The tail's damping is related to the decay of induced polarization in the reflecting surface layer of the crystal.

A Brewster incidence is chosen since near this angle the phase and amplitude of reflection coefficient change rapidly with the angle. The shorter the pulse halfwidth, the wider is an angular interval $\Delta\gamma = |\gamma - \gamma_B|$, associated with the non-zero reflection close to the Brewster angle. Thus, Campbell and Fauchet [1988] showed, that the reflection of 100 fs P-polarized IR pulse from a GaAs surface, characterized by a value of $\Delta\gamma$<0.01 rad, results in a strong reshaping of the reflected pulse, meanwhile the reshaping for a 10ps pulse becomes negligible. This transient behavior is expected to arise when the exciting pulse possesses sharp leading or tailing edges, which are shorter than the characteristic relaxation time of the system. A truncated square-shaped pulse is preferable for such "shock" excitement. For instance, Mokhtari and Chesnoy [1989] reported the observation of terahertz fluorescence transients, containing only a few oscillations with picosecond period, due to excitement of a dye solution by a femtosecond laser pulse.

II.3.2. Side by side with the reflectivity of Lorentz media, discussed above, one can consider the impulse reflection from a medium with non-local inhomogeneity-induced dispersion. An exemple of such medium consists in the now widely used " index gradient " layers. In such a case, Shvartsburg, Petite and Hecquet [2000] showed that a "waveguide – like" dispersion arises in the inhomogeneous dielectric layer with some definite distributions of normalized dielectric susceptibility $\varepsilon(z) = n_0^2 U^2(z)$. This strong inhomogeneity-induced dispersion can become a decisive effect in preserving or reshaping broadband ultrashort pulses, reflected from inhomogeneous film. Shvartsburg, Petite and Hecquet [2000] examined the broadband antireflection properties of such film in a case of normal dispersion. They showed that, for some parameters of the film the energy reflection coefficient $|R|^2$ did not exceed 5% in the frequency range $\Omega_1 < \omega < 3\Omega_1$, where Ω_1 is a characteristic cutoff frequency of the film (Fig. 12). Let us

consider, e.g., the reflection of square-shaped pulse with carrier frequency ω_0=1.77 10^{15} rad.s^{-1} (λ=1060 nm) and a total duration $2t_0$=20 fs on the film corresponding to Fig. 12. According to expression (1.7) 90% of this pulse energy are localized in the spectral range (ω_0-Δ,ω_0+Δ), here Δ=0.35 Ω_1; thus this pulse occupies a spectral range (1.65 Ω_1-2.35 Ω_1), characterized by a value of the reflection coefficient $|R|^2 \le 3\%$ .The propagation of this broadband pulse through the discussed antireflection film will be almost distortionless, though in the weak reflected field some substantial reshaping may occur.

On the contrary, an example of a strong distortion of a square-shaped pulse would arise from the passage of a broadband pulse through a thin heterogeneous film with abnormal dispersion (Fig. 13). This type of film is characterized by another characteristic frequency , here equal to Ω_2=1.6 *rad.s*$^{-1}$. The pulse under discussion differs from the previous one by a shorter wavelength (λ=800 nm) and a shorter (but still realistic) duration $2t_0$=10 fs ; so, Δ=0.38 Ω_2. Since the carrier frequency is here ω_0=2.2 Ω_2, the pulse occupies the spectral range (1.82 Ω_2-2.58 Ω_2). One can see from Fig. 13, that the reflection coefficient $|R|^2$ is diminishing in this spectral range from $|R|^2 = 0.7$ to $|R|^2 = 0.35$. Thus, the film is acting as a high-pass filter, and both the reflected and transmitted pulses will be drastically reshaped.

II.3.3. The dispersive phenomena in reflectivity of plane dielectric interfaces were discussed above by means of Fresnel formulae. However, these formulae have to be modified in order to describe the geometric dispersion, arising in the reflectivity of curvilinear surfaces, confining the dispersionless dielectric media. Owing to this effect, some rays, predicted by Fresnel's laws to be totally reflected from this interface, are reflected only partially.

The influence of such "geometric" dispersion is displayed in the reflection-refraction phenomena near by the total internal reflection (TIR) angle. Considering light incidenting from the optically denser medium onto the curved interface between two dielectric media with slightly

different refractive indices n_1 and n_2 so, that $n_1>n_2$, one can define the complement of the TIR angle θ_c by:

$$\theta_c^2 = 1 - \left(\frac{n_2}{n_1}\right)^2 \tag{2.72}$$

It follows from (2.72) that $\theta_c<<1$. Snyder and Mitchell [1973] have derived an expression for the power-transmission coefficient T in this geometry

$$T = \frac{1}{\theta_c}\left(\frac{2}{K\rho}\right)^{\frac{1}{3}}\left|Ai\left[l\exp\left(\frac{2\pi i}{3}\right)\right]\right|^{-2} \tag{2.73}$$

$$l = \left(\frac{K\rho}{2}\right)^{\frac{2}{3}}\left(\theta_c^2 - \theta_t^2\right) \tag{2.74}$$

Here θ_t is the complement of an angle of incidence g ($\theta_t=\pi/2-\gamma$), ρ is the radius of curvature in the plane of incidence, K is the wave vector in the denser medium $K = \omega n_1 c^{-1}$, Ai is the Airy function. Let us examine the grazing incidence of rays onto this interface, when the angle θ_t is small, but not zero : $1>> \theta_t >> (K\rho)^{-2/3}$. When the ray is incidenting with $\theta_t>\theta_c$, geometric optics predicts the Fresnel's value of power-transmission coefficient T:

$$T = \sqrt[4]{\left(\frac{\theta_t}{\theta_c}\right)^2 - 1} \tag{2.75}$$

for rays with $\theta_t \approx \theta_c$. However, the asymptotic forms of Airy function, given by Abramowitz and Stegun [1968]

$$\lim\left|Ai(x)\right|_{x<0,|x|>>1} = \frac{1}{2}|x|^{-\frac{1}{4}} \tag{2.76}$$

$$\lim\left|Ai(x)\right|_{x>>1} = \frac{1}{2}x^{\frac{1}{4}}\exp\left(-\frac{2}{3}x^{3/2}\right) \tag{2.77}$$

show, that eq. (2.73) can be reduced to eq. (2.75) only in the case of large negative values of argument x (2.76), when

$$\theta_t^2 - \theta_c^2 >> (K\rho)^{-2/3} \tag{2.78}$$

When the ray is incidenting with $\theta_t < \theta_c$, Fresnel's standard value *T* is zero, meanwhile the value, given by (2.73), is finite. This effect indicates some radiation energy losses due to leaky rays, penetrating to the medium n_2 . A simple expression for these losses can be obtained for leaky rays, which propagate not too close to the TIR angle: $\theta_c^2 - \theta_t^2 >> (K\rho)^{-2/3}$. Asymptotics (2.77) yields in this case the result

$$T = 4\sqrt{1-\left(\frac{\theta_t}{\theta_c}\right)^2}\,\exp\left[-\frac{2K\rho}{3}\left(\theta_c^2-\theta_t^2\right)^{3/2}\right] \qquad (2.79)$$

The values of coefficient *T* given by (2.79) are small. Thus, the efficiency of energy transfer through a curved dielectric interface by means of broadband pulses depends upon the dispersive losses. These losses, arising due to formation of leaky rays in the vicinity of TIR angle, can become important for the energy balance in bent optical fibres. Similar dispersive effects were found by Whitten, Barnes and Ramsey [1997] in propagation of pulses in the whispering-gallery modes in a narrow region around the equator of transparent homogeneous dielectric microsphere with a diameter about tens of microns. The discrete spectra of these surface modes were shown to provide coupled phenomena of modal dispersion, modal radiation losses and high quality factors $Q \approx 10^7$ of spherical optical microcavities.

II-4. **Diffraction-induced transformations of ultrashort pulses in a free space.**

There are problems, involving applications of ultrashort broadband pulses, where the spatiotemporal structure of the localized radiation must be carefully monitored. Any diffraction of these pulses from slits, apertures or gratings, existing in optical systems results in changes of the pulse's structure, since each frequency component has its own diffraction pattern. The superposition of all these diffraction patterns tends to smooth out the intensity distribution. A series of classical results in the theory of diffraction of CW trains was reconsidered recently in pulse optics. One can mention, e.g., the non-stationary generalizations of the problems of Fresnel diffraction from circular and rectangular apertures and circular opaque disk, performed

receptively by Anderson and Roychoudhuri [1998] and Gu and Gan [1996,a]. The pulse diffraction from half plane and grating was examined by Rottbrand [1997] and Ichikawa [1999].

Contrary to Section II.1, devoted to the transformations of Poisson-spectrum pulses, this chapter is centered mainly on dynamics of pulses which are initially Gaussian both in time and space. On-axis time-derivative behavior of pulses and their diffraction-induced spectral variations in the far field are discussed in the paragraph II.4.1 and II.4.3; paragraph II.4.2 is focused on the off-axis diffraction phenomena.

II.4.1. The time-dependent effects in on-axis propagation of diffracted pulse can be examined starting from the statement of this problem presented by Landau and Lifshitz [1970] (an approximation of the Helmholtz-Kirshhoff theorem using the Green's function method, applicable when the source irradiating the apperture is either punctual or spatially totally incoherent, which can be viewed as a foundation of the Huygens' principle - also see on this point Sommerfeld [1954]). The monochromatic field $E(x,y,z)$, diffracted on an opening in a flat screen, may be written in a form

$$E(x,y,z) = 2\iint E_0(x',y',0)\left.\frac{\partial G}{\partial z'}\right|_{z=0} dx'dy' \tag{2.80}$$

Here $G = (4\pi R)^{-1}\exp(ikR)$ is the Green function, $R = \sqrt{(x-x')^2 + (y-y')^2 + (z-z')^2}$ is the distance between the observation point (x,y,z) and the point of integration $(x',y',0)$ in the pupilar plane $z'=0$; the integration in (2.80) is performed over the opening. Summing over all the frequencies ω, we obtain from (2.80) the expression for the polychromatic field:

$$E(x,y,z,t) = \iiint E_0(x',y',0,\omega)\exp(-i\omega t)\left.\frac{\partial G}{\partial z'}\right|_{z=0} dx'dy'd\omega \tag{2.81}$$

Considering the far field ($kR>>1$), one can find the derivative of the Green function $\frac{\partial G}{\partial z'}$:

$$\left.\frac{\partial G}{\partial z'}\right|_{z'=0} = -\frac{ikz}{4\pi R^2}\exp(ikR) \tag{2.82}$$

Substitution of (2.82) into (2.81) yields the generalized time-dependent diffraction integral

$$E(x,y,z)=\frac{1}{c}\iint\frac{\partial}{\partial t}E_0\left(x',y',0,t-\frac{R}{c}\right)\frac{\cos\gamma}{R}dx'dy' \tag{2.83}$$

here $\cos\gamma = zR^{-1}$ is the angle between direction of observation and the normal to the screen plane. Formula (2.83) presented by Wang, Xu and Zhang [1997], contains all the information about the spatio-temporal structure of arbitrarily short diffracted pulses in the far field.

To illustrate some features of this structure let us consider first the on-axis field of a pulse with duration t_0, incidenting normally on an opaque screen with a circular opening of radius a. If the electric field E of an incident pulse is independent upon the transversal coordinates x' and y', then the field on the axis of the opening $E_{on}(z,t)$ can be easily calculated from (2.83) due to substitution

$$\begin{aligned} &dx'\,dy' = 2\pi R dR \quad ; \quad R=\sqrt{a^2+z^2} \\ &E_{on}(z,t)=\frac{1}{c}\int_0^{\sqrt{a^2+z^2}}\frac{\partial}{\partial t}\left[E_0\left(t-\frac{R}{c}\right)\right]\cos\gamma dR \end{aligned} \tag{2.84}$$

Setting $z>>a$, $\cos\gamma\approx 1$, and using $\frac{\partial}{\partial t}=-c\frac{\partial}{\partial R}$, we obtain from (2.84)

$$E_{on}(z,t)=E_0\left(t-\frac{z}{c}\right)-E_0\left(t-\frac{\sqrt{a^2+z^2}}{c}\right) \tag{2.85}$$

Thus, the pulse diffraction results in the appearance of two heteropolar pulses on the axis of the opening, which are separated by the time interval $\Delta t = a^2/2zc$. The origin of this effect is the difference in the propagation time for waves radiated by the different points of the aperture, to the on-axis observation point. These heteropolar pulses do not overlap, until the time difference Δt exceeds the pulse duration t_0. This condition determines the distance of pulse propagation without overlapping

$$z < z_0 = \frac{a^2}{2ct_0} \tag{2.86}$$

Thus, in a case a=0.1 cm, t_0=10 fs the distance z_0 is long enough (33 cm). In the far field ($z>>z_0$ or $t_0<\Delta t$) the increasing overlap of the pulses results in a weakening of the diffracted field. In this case the field E_{on} (2.85) can be written as

$$E_{on}(z,t)=\frac{a^2}{2cz}\frac{\partial}{\partial t}\left[E_0\left(t-\frac{z}{c}\right)\right] \tag{2.87}$$

which presents a general physical result : the shape of diffracted waveform in a far zone is determined by the temporal derivative of the initial waveform. This result remains valid for an arbitrary initial pulse; in particular, the homopolar Gaussian pulse (1.8) transforms in the far field into a single-cycle bipolar pulse

$$E_{on}=-\frac{E_0 a^2}{czt_0}\left(\frac{t-z/c}{t_0}\right)\exp\left[-\frac{(t-z/c)^2}{2t_0^2}\right] \tag{2.88}$$

The time-derivative diffraction-induced transformation was considered above in one the simplest cases, when the field in the opening is coordinate-independent. However, this time-differential aspect of Fresnel pulse diffraction was discussed by a series of authors, including Ziolkowsky and Judkins [1992], Gu and Gan [1996, b] and Kaplan [1998], for a pulse having an initial Gaussian distribution both in space and time

$$E(\rho,t)=E_0\exp\left(-\frac{t^2}{2t_0^2}-\frac{\rho^2}{2a^2}-i\omega t\right) \tag{2.89}$$

These researches revealed the influence of the dimensionless parameter $B=\Delta t/t_0$ on the diffracted pulse dynamics. The diffraction was found to affect greatly the laser pulse shape; when this parameter B was large. For instance, Jiang, Jacquemin and Eberhardt [1997] showed, that in a case B=40 the diffracted pulse was double-splitted; its width became more than twice that of the initial waveform, and peak power was less than half of the initial waveform peak power. This complex of non-stationary effects may have to be taken into account whenever the critical thresholds are encountered as, e.g., in non-linear optics or laser fusion.

II.4.2. The off-axis transformation of diffracted pulses with Poisson spectra, discussed above (Section II.1.1), was characterized by a pulse width increase (2.9) and a frequency red shift

(2.10). However, regardless of the shape of the broadband pulse, its lower frequency part diffracts more strongly and hence is found mostly off axis, where the higher frequencies are weaker. Similar effects were revealed in the diffraction of Gaussian pulse : Anderson and Rouchoudhuri [1998] showed an essential growth of low-pass filter function of a Gaussian pulse far from the aperture's axis. An eight-times decrease of intensity $W(\rho)$ at the pulsed beam periphery ($\rho=a$) , as compared with the axial intensity follows directly from eq. (2.12) for the Poisson-spectrum pulse; the same intensity decrease, characterized by factor 8, was computed by Aleshkevich and Peterson [1997] for a pulse consisting of one period of harmonic EM wave.
A peculiar property of off-axis radiation was shown by Bertolotti, Ferrari and Sereda [1996]: the red shift of the spectrum of the diffraction pattern for off-axis observation points is the same for the stationary polychromatic and non-stationary light sources with the same spectral composition. Moreover, generalizing the well known formula describing the intensity W of monochromatic CW train ($W=W_0$) diffracted from a slit ($-a,a$) in the far field ($R>>a$) under an observation angle γ

$$W = W_0\left(\frac{a}{R}\right)^2\left(\frac{\sin\theta}{\theta}\right)^2 \quad ; \quad \theta = \frac{a\omega_0}{c}\sin\gamma \tag{2.90}$$

Bertolotti, Ferrari and Sereda [1995] obtained the expression for spatio-temporal distribution of intensity $W_{\approx}$ of cos-Gaussian pulse, diffracted from the same slit ($-a,a$)

$$W_{\approx} = K\left(\frac{a}{R}\right)^2 |\psi|^2 \tag{2.91}$$

with

$$\psi = \frac{t_0}{\sqrt{2\pi}}\int_{-\infty}^{\infty}\exp\left[-\frac{(\omega-\omega_0)^2 t_0^2}{2} - i\omega_0 t'\right]\frac{\sin\theta}{\theta}d\omega \tag{2.92}$$

here t' is the retarded time $t-R/c$ and K is a normalization constant. The diffracted pulse, depicted on Fig. 14, proves to be split into two partially overlapping pulses, the observation angle being large enough. The shorter is the pulse, the deeper is the minimum resulting from its splitting.

The unusual properties of diffracted off-axis fields attract a special attention to potential applications of diffractive optical elements to pulsed light. Some properties of such elements can be illustrated by means of a diffraction grating, whose spatial period is comparable with the wavelength – so-called grating in the resonance domain. Comparison of diffraction of 100 fs pulsed light with central wavelength λ=800 nm and CW light with the same wavelength, performed both experimentally and numerically by Ichikawa and Minoshima [1999], revealed a significant divergence of non-zeroth diffraction sidelobes of diffracted pulses, caused by their broad spectra. The difference of diffraction angles, related to different spectral components of the pulse, could be used, as was suggested by Ito [1996], for high speed signal detection by multiple-angle spectral interferometry. Agrawal [1998] showed that a pulsed chirped diffracted beam, initially Gaussian in the transversal coordinates, did not remain Gaussian in the course of propagation, and its spot size was enhanced. Analysis of diffraction of the waveform

$$E(t) = E_0 \exp\left[-\frac{(1+iC)t^2}{2t_0^2} \right] \tag{2.93}$$

where C is the chirp parameter, revealed, that for the value C=5 the enhancement of RMS spot size was as large as 20%. Changes in the diffracted intensity were shown to be noticeable in the visible range for pulse widths below 5 fs and were increasing for large values of chirp parameter C and for pulses whose spectrum had long tails. This example of pulse spectrum-induced changes in its diffraction pattern leads us to discuss a symmetrical problem : the diffraction-induced changes in the pulse spectrum.

II.4.3. To study the spectral shifts occurring in diffraction of broadband ultrashort pulses, let us analyze the spectral intensity of an axisymmetrical beam $I_\omega(\rho, z)$ at a point with cylindrical coordinates ρ and z

$$I_\omega(\rho, z) = \left| E_\omega(\rho, z) \right|^2 \tag{2.94}$$

To find the spectral amplitude E_ω let us consider a spatially Gaussian field, incidenting normally on a circular aperture with radius *a*, located in the plane *z=0*

$$E\big|_{z=0} = E_0(t)\exp\left(-\frac{\rho^2}{2a^2}\right) \tag{2.95}$$

Solution of paraxial approximation equation (2.1), obeying the condition (2.95) ,was presented by Kaplan [1998] under the form of a Fourier transform

$$E_\omega(\rho,z) = \frac{E_0(\omega)}{1-iz/L_R}\exp\left(-\frac{\rho^2}{2a^2}\frac{1}{1-iz/L_R}\right) \tag{2.96}$$

$$E_0(\omega) = \int_{-\omega}^{\omega} E_0(t)\exp(-i\omega t)dt \tag{2.97}$$

Here $L_R = \omega a^2 c^{-1}$ is the Rayleigh range, 1-iz/L_R is the Gouy factor. Substitution of (2.97) into (2.94) brings the explicit dependence of spectral intensity I_ω upon the coordinates

$$I_\omega = \frac{\omega^2\left|E_0[\omega]\right|^2}{\omega^2+\Omega_0^2}\exp\left(-\frac{\rho^2}{a^2}\frac{\omega^2}{\omega^2+\Omega_0^2}\right) \tag{2.98}$$

$$\Omega_0 = zca^{-2} \tag{2.99}$$

To find the shift of the spectral maximum of the diffracted pulse let us consider the Gaussian modulated waveform $E_0(t)$ (2.89) and its Fourier transform

$$E_\omega = E_0 t_0\sqrt{\frac{\pi}{2}}\exp\left[-\frac{\left(\omega^2-\omega_0^2\right)}{2}t_0^2\right] \tag{2.100}$$

Substituting E_ω from (2.100) into (2.98), let us consider the on-axis spectral intensity $I_\omega(0,z)$ in the far field ($\Omega_0^2 >> \omega^2$) :

$$I_\omega(0,z) = \frac{\pi}{2}\frac{E_0^2\omega^2 t_0^2}{\Omega_0^2}\exp\left[-(\omega-\omega_0)^2 t_0^2\right] \tag{2.101}$$

The condition $\Omega_0^2 >> \omega^2$ implies that, e.g., for a radiation with wavelength λ=1060nm, passing through an opening with a=0.1 cm, expression (2.101) is valid for the distances larger than 5 cm. The maximum of intensity I_ω corresponds to the frequency

$$\omega_m = \frac{\omega_0}{2}\left[1+\sqrt{1+4(\omega_0 t_0)^2}\right] \tag{2.102}$$

Inspection of formula (2.102) shows, that the on-axis spectral maximum is blue-shifted; however, its largest value does not exceed the spectral width t_0^{-1}. Proceeding in a similar way, one can find the more complicated expressions for radius-dependent off-axis spectral shifts.

II.4.4. Unlike the aforesaid free-space effects, propagation of spatially and temporally localized waveforms in dispersive media is accompanied by an interplay of diffraction and dispersion-induced reshaping tendencies. Simultaneous action of these tendencies can lead to drastic changes of waveform's spatiotemporal parameters in the depth of dispersive media as well as to stabilization of some of these parameters. Some samples of such phenomena are listed below:

(a). Considering the propagation of a beam with a transversal spatial frequency specrtum $g_{K\perp}$,

$$E_{K_\perp \omega} = g_{K_\perp} A_\omega \exp\left[i\left(k_\perp x_\perp + k_z(\omega).z - \omega t\right)\right] \tag{2.103}$$

Porras (2001) showed that compensation of diffraction-induced and second order material dispersion effects could provide the diffraction-free and dispersion-free propagation of one fixed transversal wave vector component *p* of a broadband paraxial beam

$$k_\perp^2 = p^2 = \frac{k_0^3 k''_0}{\left(k'_0\right)^2 + k_0 k''_0} \tag{2.104}$$

where $k_0 = \omega_0 n(\omega_0) c^{-1}$ is the wavenumber corresponding to the central frequency of the beam ω_0, and k_0' and k_0'' are the coefficients of the first and second order dispersion. On the other hand, the CW monochromatic beam with the amplitude profile, given by Bessel function $J_0(u)$, $0 \le u \le 2.4$, was shown by Durnin, Micely and Eberly (1987) to propagate in free space without diffractive spreading. Unlike this, a pulsed Bessel beam, possessing some finite spectral bandwidth, is characterized by dispersive distortions. However, as it was noticed by Porras (2001), choosing the transversal profile of pulsed beam in a form $J_0(pr)$, where *p* is given by (2.104) one can cancel the second-order dispersion.

(b). The dynamics of reshaping processes in pulsed beams is governed by the competition between diffraction, increasing the pulse front curvature, and dispersion, connected with the

frequency redshift at the off - axis part of the pulse. The GVD being normal (abnormal), the red components, diffracted further from the axis, are travelling faster (more slowly), than the blue components, which are nearer to the axis. Thus, GVD results in an additional pulse front bending; the curvature radius R of the pulse front, arising from the superposition of diffraction and dispersion-induced curvatures, is given by the following expression, obtained by Porras (1999) for Gaussian pulsed beams

$$\frac{1}{R}=\left(1\mp\frac{L_R}{L_D}\right)\frac{1}{R(z)} \tag{2.105}$$

where L_R is the Rayleigh length and L_D some dispersion characteristic length. One can see from (2.105), that the normal dispersion can weaken the wavefront convexity and even transform it to a concave one. In the special case $L_D = L_R$ the wavefront remains plane.

(c). The analysis of the focusing of femtosecond pulses in lenses, performed by Bor (1988), revealed a temporal stretching of these pulses, caused by the dispersion of lens materials. A real lens with normal dispersion delays the central part of the beam as compared with the peripheral parts. Later Kempe, Stamm, Wilhelmi and Rudolph (1992) considered the possibility to cancel effectively this defect by means of achromatic lens doublet. Unlike this, Ibragimov (1995) showed that the pulse stretching could be eliminated using a Fresnel zone plate instead of one of the refractive elements in the achromatic doublet. Due to opposite dispersion of the lens and zone plate the chromatic aberration will be compensated in one focus of this combined system.

III . OPTICS OF INSTANTANEOUS MEDIA.

This Part is devoted to the amplitude, phase and frequency modulation of light interacting with media with rapidly varying optical characteristics. Such situations can be encountered in a series of hot problems in astrophysics, energy transfer through non-stationary media and optical diagnostics of ultrafast processes. The temporal variations of dielectric susceptibility $\varepsilon(t)$ under

discussion are characterized by finite relaxation times, which can become comparable with the period of probing light wave. Hence, the use of such well-known approximations of $\varepsilon(t)$ as $\delta(t)$-like model, elaborated by Felsen and Whitham [1970] or adiabatic theory, developed by Askaryan and Pogosyan [1973], as well as the perturbative approach, presented by Masoliver and Weiss [1994], cannot be used here. Some on the tendencies in ultrafast pulse reshaping, caused by finite relaxation times of $\varepsilon(t)$ for plasma and solid dielectrics, were determined by Koretsky, Kuo and Kim [1998] and Ogusu [2000] by means of numerical simulations, carried out beyond such approximations. However, the optics of instantaneous ($\varepsilon = \varepsilon(t)$) media is until now less developed than that of heterogeneous ($\varepsilon = \varepsilon(z)$) materials.

To provide some physical insight on the electromagnetics of media with time-dependent dielectric parameters, exact analytical solutions of Maxwell equations, free of any any WKB-like assumptions, are needed for such media. To stress out the crucial role of non-stationary variations of $\varepsilon(t)$, one can consider the simplest case when the relaxation dynamics of the medium is governed not by the field of the travelling wave, but by external sources, e.g., by heating, ionization or phase transitions. In particular, this approach can be related to the optics of the probing wave in the so-called "pump-probe" experiments, using ultrashort pump pulses. To tackle this problem we will use a model of non-stationary, homogeneous, non-magnetic and lossless medium, presenting a dielectric displacement **D**(t), produced by variable electric field **E**(t), by means of a scalar instantaneous dielectric function

$$\mathbf{D}(t) = \varepsilon(t)\,\mathbf{E}(t) \qquad (3.1)$$

the function $\varepsilon(t)$ can be written as

$$\varepsilon(t) = n_0^2 U^2(t) \qquad (3.2)$$

Here n_0 is the time-independent value of refractive index and the dimensionless function $U(t)$ accounts for the temporal dependence of the dielectric susceptibility. Below we study the following problems : (a) search of models of $\varepsilon(t)$, analytically solvable, inducing a "non-

stationary-induced dispersion", and related closed–form of propagation equations (§ III.1). (b). dynamical effects in the reflectivity of non-stationary media and time-dependent generalization of Fresnel formulae (§ III.2). To avoid the massive mathematics these problems will be examined for the simple case of normal incidence of a plane wave on the interface of non-stationary medium. (c). Unlike these, some polarization phenomena, pertaining to oblique incidence, are treated in § III.3.

III-1 . Non-stationary – induced dispersion in dielectrics.

Let us consider linearly polarized EM wave, incidenting normally on the boundary of half-space $z \geq 0$, filled by the non-stationary dielectric. Electric and magnetic components of this wave are linked by Maxwell equations

$$\frac{\partial E_x}{\partial z} = -\frac{1}{c}\frac{\partial H_y}{\partial t} \tag{3.3}$$

$$\frac{\partial H_y}{\partial z} = -\frac{1}{c}\frac{\partial D_x}{\partial t} \tag{3.4}$$

We have implicitly assumed that the medium is non-magnetic. The electric displacement **D** is determined in (3.1). Two models of $\varepsilon(t)$ and two related families of exact analytical solutions of the system (3.3) – (3.4), will be examined now :

III.1.1. The first way to solve the system (3.3)-(3.4) involves three steps:

a). Let us present the field components E_x and H_y via some generating function ψ_1 :

$$E_x = \frac{1}{n_0^2 U_1^2}\frac{\partial \psi_1}{\partial z} \quad ; \quad H_y = \frac{1}{c}\frac{\partial \psi_1}{\partial t} \tag{3.5}$$

Substitution of expressions (3.5) to the system (3.3)-(3.4) transforms eq. (3.3) to an identity, meanwhile the function ψ_1 is governed by eq. (3.6):

$$\frac{\partial^2 \psi_1}{\partial z^2} - \frac{n_0^2 U_1^2(t)}{c^2}\frac{\partial^2 \psi_1}{\partial t^2} = 0 \tag{3.6}$$

Introducing the new variable τ, having the dimension of a time, and the new dimensionless function F_1

$$F_1 = \frac{\psi_1}{\sqrt{U_1(t)}} \quad ; \quad \tau = \int_0^t \frac{dt_1}{U_1(t_1)} \tag{3.7}$$

we can rewrite eq. (3.6) in the form

$$\frac{\partial^2 F_S}{\partial z^2} - \frac{n_0^2}{c^2}\frac{\partial^2 F_1}{\partial \tau^2} = -\frac{n_0^2}{c^2} F_1 \left(\frac{1}{2}\frac{\partial^2 U_1}{\partial t^2} - \frac{1}{4}\left(\frac{\partial U_1}{\partial t}\right)^2 \right) \tag{3.8}$$

The temporal dependence of dielectric susceptibility still remains unknown. However, due to representation (3.8) the time-dependent coefficient is eliminated from the left side of eq. (3.8). The non-stationarity is now accounted for by the expression in brackets in the right side of eq. (3.8). Through it is not necessary, a particularly interesting class of $U_1(t)$ relates to the simplest case, when the expression in brackets in (3.8) is equal to some real constant T_1^{-2}; the quantity T_1 has the dimension of a time:

$$\frac{1}{2}\frac{\partial^2 U_1}{\partial t^2} - \frac{1}{4}\left(\frac{\partial U_1}{\partial t}\right)^2 = \frac{1}{T_1^2} \tag{3.9}$$

The function F_1 is then governed by equation with the constant coefficients

$$\frac{\partial^2 F_1}{\partial z^2} - \frac{n_0^2}{c^2}\frac{\partial^2 F_1}{\partial \tau^2} = \frac{n_0^2}{c^2 T_1^2} F_1 \tag{3.10}$$

Eq. (3.9) and (3.10) determine the temporal dependence of dielectric susceptibility $\varepsilon(t)$ and the solution of wave equations, corresponding to this model $U_1(t)$. Let us find first the model $U_1(t)$.

b. The normalized dielectric susceptibility, described by solution of eq. (3.9), obeying to condition $U_1(0) = 1$, is

$$U_1(t) = 1 + \frac{s_1 t}{t_1} + \frac{s_2 t^2}{t_2^2}; \quad s_1 = 0, \pm 1 \quad ; \quad s_2 = 0, \pm 1 \tag{3.11}$$

Here t_1 and t_2 are positive free parameters. The constant T_1^{-2} can be expressed via these parameters

$$\frac{1}{T_1^2} = \frac{s_2}{t_2^2} - \frac{s_1}{4t_1^2} \tag{3.12}$$

Depending on the values of t_1, t_2 and s_1, s_2, the function $U_1(t)$ provides flexible representations of both ascending and descending temporal dependencies of $\varepsilon(t)$. For instance, in a case where $s_1 = -1$, $s_2 = +1$, $t_2 < 2t_1$, the function $U_1(t)$ reaches its minimum (Fig. 15) at the time t_m

$$(U_1)_{\min} = U\big|_{t=t_m} = 1 - y^2 \ ; \ y = \frac{t_2}{2t_1} \le 1 \ ; \ t_m = t_2 y \tag{3.13}$$

At the time $t_c=2t_m$ this dielectric function returns to its initial value $U_1(0) = 1$

c.Solution of eq. (3.10), related to the model (3.11), can be written as a travelling wave

$$F_1 = A_1 \exp i(q_1 z - \omega\tau)$$
$$q_1 = \frac{\omega n_0}{c} N_1 \quad ; \quad N_1^2 = 1 - \frac{1}{(\omega T_1)^2} \tag{3.14}$$

Substitution of (3.14) to (3.7) yields the generating function

$$\psi_1 = A_1 \sqrt{U_1(t)} \exp i(q_1 z - \omega\tau) \tag{3.15}$$

Here A_1 is a normalization constant. Finally, substitution of (3.15) into the definitions (3.5) brings the expressions for field components inside the non-stationary medium (3.11):

$$E_x = \frac{iA_1\omega N_1}{cn_0} [U_1(t)]^{-3/2} \exp i(q_1 z - \omega\tau) \tag{3.16}$$

$$H_y = \frac{iA_1\omega}{cn_0} [U_1(t)]^{-1/2} \left(1 + \frac{i}{2\omega}\frac{\partial U_1}{\partial t}\right) \exp i(q_1 z - \omega\tau) \tag{3.17}$$

Before discussing the properties of this field, let us consider another family of exactly solvable models for the Maxwell equations (3.3)-(3.4).

III.1.2. The second method of solution of the system (3.3)-(3.4) is following the same scheme as in III.1.1; however, another generating function is chosen.

Presenting the EM field components via the generating function

$$E_x = \frac{1}{c}\frac{\partial \psi_2}{\partial t} \quad ; \quad H_y = \frac{\partial \psi_2}{\partial z} \tag{3.18}$$

we will transform eq. (3.3) to an identity; eq. (3.4), which determines the function ψ_2, will be written as

$$\frac{\partial^2 \psi_2}{\partial z^2} - \frac{n_0^2 U_2^2(t)}{c^2}\frac{\partial^2 \psi_2}{\partial t^2} = \frac{n_0^2}{c^2}\frac{\partial U_2^2}{\partial t}\frac{\partial \psi_2}{\partial t} \tag{3.19}$$

Using the variable τ(3.7) and introducing the new function F_2 in a form:

$$F_2 = \psi_2 \sqrt{U_2(t)} \tag{3.20}$$

one can eliminate the unknown dependence $U_2(t)$ from the left side of eq. (3.19)

$$\frac{\partial^2 F_2}{\partial z^2} - \frac{n_0^2}{c^2}\frac{\partial^2 F_2}{\partial \tau^2} = -\frac{n_0^2}{c^2}F_2\left(\frac{U_2}{2}\frac{\partial^2 U_2}{\partial t^2} + \frac{1}{4}\left(\frac{\partial U_2}{\partial t}\right)^2\right) \tag{3.21}$$

Equating the expression in brackets (3.21) to some real constant

$$\left(\frac{U_2}{2}\frac{\partial^2 U_2}{\partial t^2} + \frac{1}{4}\left(\frac{\partial U_2}{\partial t}\right)^2\right) = -\frac{1}{T_2^2} \tag{3.22}$$

will reduce eq. (3.21) to a form, similar to (3.10)

$$\frac{\partial^2 F_2}{\partial z^2} - \frac{n_0^2}{c^2}\frac{\partial^2 F_2}{\partial \tau^2} = \frac{n_0^2}{c^2 T_2^2}F_2 \tag{3.23}$$

To find the model $U_2(t)$ from (3.22) let us introduce the new function $Q = \sqrt{U_2}$; using the variable τ(3.7), we will find from (3.22)

$$\frac{\partial^2 Q}{\partial \tau^2} + \frac{Q}{T_2^2} = 0 \tag{3.24}$$

Subject to the sign of parameter T_2^2 the function $U_2(\tau)$ can be expressed via the solution of (3.24) in two different forms:

$$U_2(\tau) = \left[\cos\left(\tau/T_2\right) + M_1 \sin\left(\tau/T_2\right)\right]^2 \qquad T_2^2 > 0 \tag{3.25}$$

$$U_2(\tau) = \left[ch\left(\tau/T\right) + M\ sh\left(\tau/T\right)\right]^2 \qquad T^2 = -T_2^2 > 0 \tag{3.26}$$

The special case, when the right side of eq. (3.22) is equal to zero, is not examined here.

The temporal dependencies $U_2(\tau)$ are presented in (3.25)-(3.26) by means of variable $\tau = \tau(t)$. To present the dependence of the family of models $U_2(t)$ upon the physical time, one has to solve these equations with respect to τ and to substitute the dependence $\tau = \tau(U_2)$ into the definition of (3.7). Thus, in a case (3.26) one can find, supposing $M^2<1$:

$$\frac{\tau}{T} = arcch\left(\sqrt{\frac{U_2}{1-M^2}}\right) - arcch\left(\frac{1}{\sqrt{1-M^2}}\right) \tag{3.27}$$

Combining formulae (3.27) and (3.7) we will obtain an equation, governing the temporal dependence $U_2(t)$, containing two free parameters T and M

$$\frac{dU_2}{dt} = \mp\frac{2}{T}\sqrt{1-\frac{1-M^2}{U}} \tag{3.28}$$

The signs – and + in (3.28) relate to the descending and ascending branches of the function. The descending solution of (3.28) describes the decrease of function $U_2(t)$ from an initial value of 1 towards its minimum value $U_{\min} = 1 - M^2$ during a time t_m

$$\frac{t}{T} = \frac{1}{2}\left\{M - \sqrt{U_2(U_2 + M_1^2 - 1)} + \left(1-M^2\right)\left[arcch\left(\frac{1}{\sqrt{1-M^2}}\right) - arcch\left(\sqrt{\frac{U_2}{1-M^2}}\right)\right]\right\} \tag{3.29}$$

$$\frac{t_m}{T} = \frac{1}{2}\left\{M + \left(1-M^2\right)\left[arcch\left(\frac{1}{\sqrt{1-M^2}}\right)\right]\right\} \tag{3.30}$$

Dividing eq. (3.29) by eq. (3.30) one can eliminate the free parameter T, replacing it by the characteristic evolution time t_m:

$$\frac{t}{t_m} = 1 - \frac{\sqrt{U_2(U_2 + M_1^2 - 1)} + \left(1-M^2\right)arcch\left(\sqrt{U_2/\left(1-M^2\right)}\right)}{M + \left(1-M^2\right)arcch\left(1/\sqrt{1-M^2}\right)} \tag{3.31}$$

Unlike (3.11), this model $U_2(t)$ is more easily presented via an inverse function $t = t(U_2)$. The ascending branch, related to the growth of function $U_2(t)$ from its minimum $U_{\min} = 1 - M^2$ up to the value $U=1$ can also be found starting from eq. (3.28). Both these branches are shown on Fig. 15.

Substitution of solution of eq. (3.23), written in a form of travelling wave, similar to (3.14)-(3.15), to the expression (3.20) yields the generating function

$$\psi_2 = \frac{A_2 \exp i(q_2 z - \omega\tau)}{\sqrt{U_2(t)}} \; ; \; q_2 = \frac{\omega n_0}{c}\sqrt{1-(\omega T)^{-2}} = \frac{\omega n_0}{c} N_2 \tag{3.32}$$

The field components E_x and H_y can be found from (3.18):

$$E_x = \frac{iA_2\omega}{cn_0}[U_2(t)]^{-1/2}\left(1 - \frac{i}{2\omega}\frac{\partial U_2}{\partial t}\right)\exp i(q_2 z - \omega\tau) \tag{3.33}$$

$$H_y = \frac{iA_2\omega N_2}{cn_0}[U_2(t)]^{-3/2}\exp i(q_2 z - \omega\tau) \tag{3.34}$$

The derivative $\frac{\partial U_2}{\partial t}$ is given in (3.28).

Thus, we obtained, with $U_1(t)$ and $U_2(t)$, two models for the non-stationary dielectric susceptibility allowing to obtain exact solutions of the propagation equation in a non stationary dielectric, in the sense that no "slowly varying envelope" assumption has to be made. The application of these models can be exemplified by the problem of probing wave reflection from a dielectric, in which the carrier density grows steeply due to ionization, induced by a high-power laser beam. It is convenient to present the instantaneous dielectric susceptibility by means of functions

$$\varepsilon = \varepsilon_L\left[1 - \frac{\Omega_0^2 K(t)}{\omega^2}\right] = \varepsilon_L\left[1 - \frac{\Omega_0^2}{\omega^2}\right]U^2(t) \tag{3.35}$$

where ε_L is the lattice dependent part of the dielectric susceptibility, $\Omega_0^2 = e^2 N_0 (m\varepsilon_L)^{-1}$, and $U(t)$ will be approximated by a function of the form (3.11). N_0 is an unperturbed electron density, function $K(t)$ satisfies the condition $K(0)=1$. Let us consider a "symmetrical" regime, where the ionization reaches its peak $N_m=N_0K_m$ in a time t_m and returns thereafter to the initial value in the same time interval. This regime relates to the concave profile of U_1^2, depicted on Fig. 15. The time scales t_1 and t_2 in U_1^2 can be found from the condition at time $t=t_m$ (3.13)

$$U_m = U_1\big|_{t=t_m} = \left(1-y^2\right)^2 = \left(1-\frac{\Omega_0^2 K_m}{\omega^2}\right)\left(1-\frac{\Omega_0^2}{\omega^2}\right)^{-1} \tag{3.36}$$

Using the value K_m one can calculate from (3.36) the parameter y and express the time scales t_1, t_2 and T_0 via the time interval t_m

$$t_1 = \frac{t_m}{2y^2}\ ;\ t_2 = \frac{t_m}{y}\ ;\ T_0 = \frac{t_m}{y\sqrt{1-y^2}} \tag{3.37}$$

This approach will be used below for analysis of instantaneous plasma reflectivity.

III.1.3. The expressions for EM fields (3.16)-(3.17) and (3.33)-(3.34), propagating in the non-stationary media, described by both U_1 and U_2 models, contain the phase factor $\exp i\left(qz-\omega\tau\right)$, expressed using variable τ: in this "τ-space", the spatiotemporal structure of the discussed EM fields resemble that of travelling harmonic waves with time-dependent amplitudes. Let us analyze the amplitude–phase structure of field components (3.16)-(3.17), emphasizing some peculiarities of this structure, originating from the strong non-stationarity of the medium they travel in :

(a). The wave propagation is characterized by non-stationarity induced dispersion, described by factor N (3.15). The "concave" temporal profile of dielectric susceptibility, depicted on Fig. 15, gives rise to normal dispersion ($N = \sqrt{1-\left(\omega T\right)^{-2}}$); this waveguide – like formula shows the appearance of non-stationarity – induced cut-off frequency $\Omega = T^{-1}$. On the contrary, a convex profile of $U(t)$ gives rise to abnormal dispersion ($N = \sqrt{1+\left(\omega T\right)^{-2}}$) , and the cut-off effect does not arise in this case.

(b). The electric component (3.16) can be viewed as a non-stationary wave, travelling in the (z,τ) space with a constant phase velocity. However, in the physical space (z,t) the phase velocity is varying in time. These variations give the rise to a drastic reshaping of waveforms. To determine this reshaping, one has to find the explicit expression for parameter τ (3.7). For simplicity, let us

consider the case where a wave front is incidenting on the boundary at the beginning of temporal variation of dielectric susceptibility $t=0$. The result of integration (3.7) in this case is

$$\frac{\tau(t)}{T_0} = Arctg\left(\frac{t/T_0}{1 - ty^2/t_m}\right) \tag{3.38}$$

The duration of perturbation of dielectric susceptibility is $t_c=2t_m$. At any time $t_f \leq t_c$ the position z_0 of the front of electric waveform (3.16) is determined by the equation

$$qz_0 - \omega\tau(t_f) = 0 \tag{3.39}$$

Let us characterize by its phase difference φ with the front edge a waveplane crossing position z_0 at a later time t_d ($t_f < t_d \leq t_c$). Given the constant phase velocity of the wave in the perturbed medium in the "τ-space", one has :

$$\tau(t_d) - \tau(t_f) = \varphi/\omega \tag{3.40}$$

which can be used to determine the unknown t_d. One can then find the amplitude modulating factor with expression (3.16). Propagation through the area with decreased dielectric susceptibility results in an increase of the electric strength amplitudes. Since the temporal perturbation stops at time t_c, the parts of waveform, incidenting on the plane $z=0$ at times $t>t_c$ are travelling in the medium without reshaping. Thus, only the leading front of the waveform proves to be distorted (Fig. 16).

(c).The non-stationarity induced dispersion is determined by the finite relaxation time of instantaneous dielectric susceptibility t_c. When this time is increasing, this dispersion is vanishing. The quantities N, U and τ tend to the values $N=1$, $U=1$ and t. The fields E_x and H_y are approaching that of a sinusoidal waves in a stationary dielectric.

(d). Finally, it should be mentioned that the results presented here in the case of normal incidence can be generalized to an arbitrary angle of incidence. In such a case, model (3.11) only applies to a P-polarized incident field, and model (3.26) to a S-polarized one. In the case of normal incidence, both polarizations coincide, and it is natural that both models apply. In the general case, the only time dependence which simultaneously applies to both polarizations (with

the requirement of a constant right-hand term in eqs. (3.8) and (3.21), which is not strictly necessary) should obey the condition $\partial^2 U/\partial t^2 = 0$, and thus are of the type $U(t) = 1 \pm t/t_0$. Note that this model is obviously contained in expression (3.26), but also in (3.11), with *M=1*

III.2 Dynamical regime in reflectivity of non-stationary dielectrics.

Electromagnetic fields in the non-stationary dielectrics were shown to depend not only upon the current values of time-dependent dielectric susceptibilities $\varepsilon(t)$, but also upon the temporal derivatives of $U(t)$ - see, e.g., eq. (3.16)-(3.17) and (3.33)-(3.34). These derivatives determine the non-stationary phases of reflected and refracted waves.

To find the generalized Fresnel formulae, describing these dynamical phase effects, let us examine the problem of reflection of a linearly polarized EM wave with frequency ω on the non-stationary dielectric, filling the half-space *z>0.* Using the continuity conditions for the fields at the interface, one can obtain the reflection coefficients (here in a general case, for both S and P-polarizations, with an arbitrary incidence angle γ) :

$$R_S = \frac{\cos\gamma - \sqrt{n_S^2 - \sin^2\gamma}}{\cos\gamma + \sqrt{n_S^2 - \sin^2\gamma}} \quad ; \quad n_S = n_0 U(t) N_S \left(1 - \frac{i}{2\omega}\frac{\partial U}{\partial t}\right)^{-1} \tag{3.40}$$

$$R_P = \frac{n_0^2 U^2(t)\cos\gamma - \sqrt{n_P^2 - \sin^2\gamma}}{n_0^2 U^2(t)\cos\gamma + \sqrt{n_P^2 - \sin^2\gamma}} \quad ; \quad n_P = n_0 U(t) N_P \left(1 + \frac{iU_t}{2\omega}\right)^{-1} \tag{3.41}$$

where we used a complex angle of refraction β

$$\sin\gamma = n_{S,P}\sin\beta \tag{3.42}$$

Note that these results are general and apply under the only condition that eq. (3.8) or (3.21) have a constant right hand side. One important remark concerns the fact that the laws of reflection (non-stationary counterparts of the Descartes/Snell and Fresnel laws) depend on a "reflection" index ($n_{S,P}$) which differs from the refractive index ($N_{S,P}$, which determine the propagation inside the dielectric, and account for the non-stationarity induced dispersion described above), which are themselves different from the "instantaneous refractive index" -

$n(t)=n_0U(t)$. Let us now come back to the case of a normal incidence, in which S and P polarizations coincide, and use a very simple dielectric constant model, encompassing both cases developped above, i.e.

$$U(t) = 1 - t/t_0 \tag{3.43}$$

which allows simple calculations, but nevertheless yields results which can be generalized to the two models of U discussed above, at the expense of some increased algebraic complexity only. Here, one has $N_S^2 = N_P^2 = 1 + (2\omega t_0)^{-2} = 1 + 1/\varphi_0^2$. The real and imaginary parts of the reflection coefficient then write.

$$Re(R) = \frac{N(1 - n^2(t))}{N(1 + n^2(t)) + 2n(t)} \tag{3.44}$$

$$\mathrm{Im}(R) = \frac{-2in(t)}{\varphi_0[N(1 + n^2(t)) + 2n(t)]} \tag{3.45}$$

Yielding intensity reflection coefficient $|R|^2$ and phase Φ

$$|R|^2 = \frac{N^2[1 - n^2(t)]^2 + 4n^2(t)/\varphi_0^2}{(N[1 + n^2(t)] + 2n(t))^2} \tag{3.46}$$

$$\Phi = Arctg\left[\frac{-2n(t)}{\varphi_0 N[1 - n^2(t)]}\right] \tag{3.47}$$

In a limiting case, when the non-stationary vanishes ($t_0,\varphi_0\rightarrow\infty$), $N\rightarrow 1$, $Im(R)$ vanishes, meanwhile $Re(R)$ is reducing to the usual Fresnel formula. It is interesting to compare them to a "quasistationary" approximation in which one would simply use the regular Fresnel formulae using the instantaneous value of the "normal" refractive index, that is to say (we consider the case of a positive dielectric constant). The Fresnel reflection coefficient then writes

$$R = \frac{1 - n(t)}{1 + n(t)} \tag{3.48}$$

which, first, has no imaginary part, and, second, has a real part, quite different from that of eq. (3.48). Fig. 17 allows to evaluate the errors that result from the use of the quasistationary approximation. The intensity reflection coefficient (3.46) and the phase (3.47) are compared to

that obtained from the quasistationary value (3.48). There are very significant differences up to values of φ_0 of a few units. For $\varphi_0 = 5$ the intensity reflection coefficient is almost equal to the quasistationary value, but some significant effects are still visible on the phase up to $\varphi_0 = 10$. The phase of the reflected light therefore seems to be a much more sensitive test of such effects than the intensity reflection coefficient.

It is also interesting to consider the case of a negative dielectric constant, arising in the area $t>t_0$. $\varepsilon(t)$ can be presented in this area using the following function

$$U(t) = i\left(\frac{t}{t_0} - 1\right) \tag{3.49}$$

which provides continuity of the dielectric susceptibility and its temporal derivatives at time $t=t_0$ With such a $U(t)$, the modulus of the reflection is equal to 1 if (and if only) $\varphi_0 > 1$. In such a case, the phase of the reflection coefficient is found equal to :

$$\Phi = Arctg\left[\frac{2\varphi_0\left(t/t_0 - 1\right)\left(\varphi_0^2 - 1\right)^{1/2}}{\varphi_0 + 1 - \left(t/t_0 - 1\right)^2(\varphi_0 - 1)}\right] \tag{3.50}$$

However, when $\varphi_0 < 1$, one finds a real reflection coefficient, equal to :

$$R = \frac{\varphi_0^2 - \left(t/t_0 - 1\right)\left(1 - \varphi_0^2\right)^{1/2}}{\varphi_0^2 + \left(t/t_0 - 1\right)\left(1 - \varphi_0^2\right)^{1/2}} \tag{3.51}$$

smaller than unity, as it should, which brings in the conclusion that an ultrafast-varying medium of negative dielectric constant may not be totally reflective! Quite normally, when $\varphi_0 \to 1$(-), The reflection coefficient (3.51) tends toward unity, whereas when $\varphi_0 \to 1$ (+), the phase (3.50) tends toward zero, so that continuity between the two regimes is perfect.

These phenomena, which cannot be described by “quasistationary” expression (3.46), illustrate the importance of dynamical effects in the reflectivity of instantaneous dielectrics.

It should be mentioned, that the dielectric susceptibility in the model (3.43) tends towards zero, when $t \to t_0$; in this case, which is experimentally realizable, one finds that the fields in the medium - (3.33) and (3.34) - take arbitrarily high values, which questions the validity of the linear approximation used in the definition of the displacement current (3.1). It should be noted, however, that the strong effects in reflectivity, shown on Fig. 17, do not particularly occur in the region where ε vanishes, so that this limitation of the model does not affect the above conclusions. Moreover, one would obviously have to take into account in such a case the dissipation processes that occur in any real physical situation. Whether they would be strong enough to reduce the field to values acceptable for a linear theory cannot be ascertained at present, but it is worth showing how dissipation can be included in the above theory simply enough by using complex time scales, describing the non-stationary complex dielectric susceptibility. Considering the simple generalization of the model (3.43), describing both time-dependent refraction and attenuation

$$U(t) = 1 - \frac{t}{t_0 + it_1} \tag{3.52}$$

one can present the variable τ (3.7) in a complex form

$$\begin{aligned} &\tau = Re(\tau) + iIm(\tau) \\ &Re(\tau) = t_0 D - t_1 M \;;\; Im(\tau) = t_1 D + t_0 M \\ &D = \frac{1}{2}\ln\left[\left(1 - \frac{tt_0}{t_0^2 + t_1^2}\right)^2 + \left(\frac{tt_1}{t_0^2 + t_1^2}\right)^2\right] ;\; M = Arctg\left(\frac{tt_1}{t_0^2 + t_1^2 - tt_0}\right) \end{aligned} \tag{3.53}$$

Substitution of (3.52) and (3.53) into the field representation (3.16)-(3.17) provides finite values for all field components at any time. The non-stationary reflectivity of a medium (3.53) is determined again by eq. (3.45)-(3.46), parameter t_0 being replaced by $t_0 + it_1$; herein the expressions for φ_0 and N become complex:

$$\varphi_0 = 2\omega(t_0 + it_1) \;;\; N = \sqrt{1 + [2\omega(t_0 + it_1)]^{-2}} \tag{3.54}$$

These results illustrate the dynamical regimes of reflectivity of non-stationary dielectrics, which depend essentially upon the relaxation times of their dielectric susceptibility, for the

normal incidence (except for the general expressions (3.44)-(3.46) which include the case of an oblique incidence). Some dynamical effects for the inclined incidence are considered below.

III.3**. Spectral distortions of waves reflected from the instantaneous dielectric.**

Time-dependent phase shift of the reflected wave $\Phi(t)$ is presented in (3.51) for the normal incidence. These temporal variations of $\Phi(t)$ can be considered as the spectral distortions of reflected wave

$$\Delta\omega(t) = -\frac{\partial\Phi}{\partial t} \tag{3.55}$$

Unlike the well known Doppler frequency shifts, pertaining to the reflectivity of moving media, the spectral shifts (3.55) find their origin in the temporal variations of the dielectric susceptibility of motionless medium. So they should rather be viewed as a phase modulation, not self induced in this particular case where the modifications of the dielectric susceptibility are not due to the EM field we study. These spectral shifts can be quite significant in the case of oblique incidence of the EM wave. If we consider the case of a P-Polarized incident beam, the expression of the reflection coefficient is given in (3.46). One has to emphasize again the dependence of reflectivity upon both the current value of dielectric susceptibility and its temporal derivative. It is interestingy to illustrate some particular features of time-dependent reflection and spectral distortions of reflected wave (Fig. 18), corresponding to the descending branch of model (3.11), (i) The amplitude of reflection coefficient $|R_P|$ has no zero-crossing point for any angle of incidence γ. Thus, the situation $|R_P| = 0$, well known for the reflection of P-polarized waves from stationary lossless dielectrics under some angles of incidence (Brewster effect), does not appear for non-stationary dielectics (Fig. 18a). (ii) The waves reflected from the medium with decreasing dielectric susceptibility are red shifted (Fig. 18b).

CONCLUSION.

The analysis of ultrafast transient optical problems was centered above on some phenomena of spatiotemporal dynamics of ultrashort pulses, travelling in stationary dielectric media, and interactions of CW trains with non-stationary dielectrics. Paraxial propagation of ultrashort pulses in the free space was shown to provide a series of coupled instantaneous effects – spectral distortions, waveform reshaping and polarization reversal. Localization of pulses in a plane, orthogonal to the direction of propagation, results in the complicated interplay of diffractive and dispersive effects. Several analytical models of interaction of ultrashort pulses with media, characterized by material and inhomogeneity – induced dispersion were considered both in frequency and time domain.

Generalization of Fresnel formulae for reflectivity of instantaneous dielectrics, based on exact analytical solutions of Maxwell equations for these media, has been presented. The dynamical regimes of instantaneous reflectivity, illustrating the decisive influence of non-stationary-induced dispersion on amplitude, phase and spectral distortions of reflected waves, were considered.

Optics of transient waveforms is nowadays a hot and rapidly expanding branch of electromagnetics, and it is noteworthy to stress out some problems, which remain opened till now:

(i). Optics of nonstationary inhomogeneous media, in which the dielectric susceptibility of the medium is varying in time and space simultaneously. The simplest model, presented by Stenflo, Shvartsburg and Weiland [1997], revealed the complicated interplay between inhomogeneity – and non-stationary-induced dispersive phenomena, when the temporal and spatial perturbations of $\varepsilon(t)$ are supposed to be independent. However, the analysis of coupled spatial-temporal variations of $\varepsilon(t)$ is in need.

(ii). Search of optimized regimes of propagation of directed pulsed beams of anharmonic waveforms through non-stationary media.

(iii). All the above mentioned problems were investigated for media with well determined distributions of dielectric parameters. However, the non-stationary optics of random media is still waiting for its researchers. This problem is in particular relevant to the use of ultrashort pulses in the field of atmospheric optics.

Acknowledgements.

The authors are much obliged to Professors G. Agrawal, J. Eberly, S. Haroche, A. Migus, L.Vazquez and E.Wolf for their immutable interest in this work and many valuable discussions.

References

Aaviksoo, J., J. Kuhl, 1989, IEEE J. Quant. Electron. **25**, 2523.

Aberg, I., G. Kristensson, D. Wall, 1996, J. Math. Phys. **37**, 2229.

Abramowitz, M., I. Stegun, 1968, Handbook of Mathematical Functions, Dover Publications, Section 10.4.

Agrawal,G., J. Birman, D. Pattanayak, A. Puri, 1982, Phys. Rev. B **25**, 2715.

Agrawal, G., 1995, Non – Linear Fiber Optics, Academic Press, 2nd ed., 39.

Agrawal, G., 1998, Opt. Comm. **157**, 52.

Akimoto, K., 1996, J. of the Phys. Soc. of Japan **65**, 2020.

Aleshkevich, V., V. Peterson, 1997, JETP Letters **66**, 323.

Anderson, J., C. Roychoudhuri, 1998, J. Opt. Soc. Am. A **15**, 496.

Askaryan, G., V. Pogosyan, 1973, JETP, 117.

Bateman, H., 1955, *The Mathematical Analysis of Electrical and Optical Wave Propagation on the Basis of Maxwell Equations*, Dover Publications, pp. 27 – 30.

Baum, C., E. Rothwell, K. Chen, D. Nyquist, 1991, Proc. IEEE **79**, 1481.

Bertolotti, M., A. Ferrari, L. Sereda, 1995, J. Opt. Soc. Am. B **12**, 1519.

Bor, Z., 1988, J. Modern Optics **35**, 1907.

Brabec, T., F. Krausz, 1997, Phys. Rev. Lett. **78**, 3282.

Brittingham, J., J. Appl. Phys. **54**, 1179.

Bromage, J., S. Radic, G. Agrawal, C.Stroud Jr, P. Fauchet, R. Sobolewski, 1998, J. Opt. Soc. Am. B **15**, 1953.

Campbell, I., P. Fauchet, 1988, Opt. Lett. **13**, 634.

Code, D., 1999, Appl. Phys. Lett. **75**, 3959-3961

Dijaili, S., A. Dienes, J. Smith, 1990, IEEE J. Quant. Electron. **26**, 1158

Dorrer, C., M, Joffre, 2001, C.R. Acad. Sci. Paris, t.**2**, Serie IV, 1415-1426

Durnin, J., J. Micely, J. Eberly, 1987, Phys. Rev. Lett. **58**, 1499.

Einziger, P., S. Raz, 1987, J. Opt. Soc. Am. A **4**, 3.

Felsen, L., J. Whitham, 1970, IEEE Trans. AP-**18**, 272.

Feng,S., H. Winful, 1998, Opt. Lett. **23**, 385.

Feng, S., H. Winful, R. Hellwarth, 1999, Phys. Rev. E **59**, 4630.

Fittinghoff, D. N., A. C. Millard, J. A. Squier, M. Muller, 1996, Opt. Lett. **21**, 884-886

Grischkowsky, D., S. Keiding, M. van Exter, C. Fattinger, 1990, J. Opt. Soc. Am. B **7**, 2006.

Gu, M., X. Gan, 1996 a, Opt. Comm. **125**, 1.

Gu, M., X. Gan, 1996 b, J. Opt. Soc. Am. A **13**, 771.

Hu, B., M. Nuss, 1995, Opt. Lett. **20**, 1716.

Hillion, P., 1983, Acta Math. Appl. **30**, 35.

Iaconis, C., I. A. Walmsley, 1998, Otpics Lett., **23**, 792-794

Ibragimov, E., 1995, Appl. Opt. **34,** 7280.

Ichikawa, H., 1999, J. Opt. Soc. Am. A **16**, 299.

Ichikawa, H., K. Minoshima, 1999, Opt. Comm. **163**, 243.

Ito, F., 1996, IEEE Journal of Quantum Electronics **32**, 519.

Jiang, Z., R. Jacquemin, W. Eberhardt, 1997, Appl. Opt. **36**, 4358.

Jones, R., D. You, F. Bucksbaum, 1993, Phys. Rev. Lett. **70**, 1236.

Kane, D. J., R. Trebino,1993, Opt. Lett. **18**, 823

Kaplan, A., 1998, J. Opt. Soc. Am. B **15**, 951.

Karlsson, M., A. Hook, 1994, Opt. Comm. **104**, 303.

Keiding, S., 1994, Comments Mol. Phys. **30**, 37.

Kempe, M., U. Stamm, B. Wilhelmi, W. Rudolph, 1992, J. Opt. Soc. Am. B **9**, 1158.

Kiselev, A., M. Perel, 2000, Journal of Math. Phys. **41**, 1934.

Koretsky, E., S. Kuo, J. Kim, 1998, J. Plasma Phys. **59**, 315.

Landau L., Lifshitz E., 1970, in "*Fields Theory"*, (ed. Mir-Moscow), section 59,

Lepetit, L., G. Cheriaux, M. Joffre, 1995, J. Opt. Soc. Am. B **12**, 2467-2474

Ma, J., I. Ciric, 1992, Radio Science **27**, 561.

Maine, P., D. Strickland, P. Bado, M. Pessot, G. Mourou, 1988, IEEE J. Quantum Electron. **24**, 398

Maradudin, A., 1999, Opt. Lett. **24**, 37.

Masoliver, J., G. Weiss, 1994, Phys. Rev. E **49**, 3852.

Matsui, Y, M. D. Pelusi, A. Suzuki, 1999, IEEE Photonics Technology Lett., **11**, 1217-1219

Mattuschek, N., L. Gallmann, D. H. Sutter, G. Steinmeyer, U. Keller, 2000, Appl. Phys. B **71**, 509

McGowan, R., G. Gallot, D. Grischkowsky, 1999, Opt. Lett. **24**, 1431.

Melamed, B., L. Felsen, 1998, J. Opt. Soc. Am. B **15**, 1268.

Mokhtari, A., J. Chesnoy, 1989, IEEE Journal of Quantum Electronics **25**, 2528.

Nodland, B., 1997, Phys. Rev. E **55**, 3647.

Ogusu, K., 2000, J. Opt. Soc. Am. B **17**, 1894.

Paul, P.M., E. S. Toma, P. Breger, G. Mullot, F. Augé, P. Balcou, H. G. Muller, P. Agostini, 2001, Science **292**, 1989-1992

Porras, M., 1998, Phys. Rev. E **58**, 1086.

Porras, M., 1999, J. Opt. Soc. Am. B **16**, 1468.

Porras, M., 1999, Phys. Rev. A **60**, 5069.

Porras, M., 2001, Opt. Lett. **26**, 847.

Qian, Y., E. Yamashita, 1991, IEEE Transactions on Microwave Theory and Techniques **39**, 924.

Quere, F., S. Guizard, P. Martin, G. Petite, O. Gobert, P. Meynadier, M. Perdrix, 1999, Appl. Phys. B **68**, 459.

Rottbrand, K., 1998, Z. Angew. Math. Mech. **78**, 321.

Salliéres, P., A. L'Huillier, P. Antoine, M. Lewenstein, 1999, in "*Advances in Atomic, Molecular and Optical Physics*" B. Bederson, H. Walther eds. (Academic Press, New York,) vol **41,**, p. 83

Schins, J. M., P. Breger, P. Agostini, R. C. Constantinescu, H. G. Muller, G. Grillon, A. Antonetti, A. Mysyrowisz, 1994, Phys. Rev. Lett. **73**, 2180

Shvartsburg, A., 1999, *Impulse Time - Domain Electromagnetics of Continuous Media*, Birkhauser, Boston, pp. 5–6.

Shvartsburg, A., G. Petite, P. Hecquet, 2000, J. Opt. Soc. Am. A **17**, 2267.

Smith, P., D. Auston, M. Nuss, 1988, IEEE J. Quantum Electronics **24**, 255.

Snyder, A., D. Mitchell, 1973, Electronics Letters **9**, 609.

Sommerfeld A., 1954, in "*Optics"*, (New York, Academic Press), p. 199

Stenflo, L., A. Shvartsburg, J. Weiland, 1997, Contrib. Plasma Phys. **37**, 393.

Szipöcs, R., K. Ferencz, C. Spielmann, F. Krausz, 1994, Opt. Lett. **19**, 201

Tang, N., L. Sutherland, 1997, J. Opt. Soc. Am. B **14**, 3412.

Wang, Z., Z. Xu, Z. Zhang, 1997, Opt. Lett. **22**, 354.

Weber H. P., E. Mathieu, K. P. Meyer, 1966, J. Appl. Phys., **37**, 3584-3586

Whitten, W., J. Barnes, J. Ramsey, 1997, J. Opt. Soc. Am. B **14**, 3424.

Weling, A., B. Hu, N. Froberg, D. Auston, 1994, Appl. Phys. Lett. **64**, 137.

Wolf, E., 1986, Phys. Rev. Lett. **56**, 1370.

Wolf, E., 1987, Nature **326**, 363.

Wu, T., 1985, J. Appl. Phys. **57**, 2370.

You, D., R. R. Jones, P. H. Bucksbaum, D. R. Dykaar, 1993, Opt. Lett. **18**, 290

Ziolkowsky, R., J. Judkins, 1992, J. Opt. Soc. Am. B **9**, 2021.

Figure Captions.

Fig. 1. (Fig. 1a) : Asymmetrical pulse 1 and symmetrical transform-limited (TL) pulse 2, plotted vs the normalized time $u=t/t_0$ characterized by the same normalized spectral envelope (Fig. 1b) : spectral envelope (curve 3) $y = F(x)/F(0)$, $m=\varphi(x)/\pi$, $x=t_0(\omega-\omega_0)$. Unlike the spectral phase φ of pulse 1, shown by curve 4, the frequency dependence of phase of TL pulse (curve 5) is linear.

Fig.2. (a) Laguerre envelops $L_0(x)$: —□—, $L_1(x)$: —○—, $L_2(x)$: —◊— , (b): unipolar $F_1(x) = L_0(x) - L_1(x)$: —□— and bipolar $F_2(x) = L_0(x) - L_2(x)$: —○— waveforms, $x=t/t_0$

Fig. 3. Poisson – spectrum pulses (1.20) for the values of parameter $m=1$ (curve 1) and $m=2$ (curve 2) are plotted vs the normalized time $x=t/t_0$

Fig. 4. Temporal waveforms of electric e_3 (solid line) and magnetic h_3 (dashed line) components of non-sinusoidal EM field on the interface of plasma – like medium (2.68) are plotted vs the normalized time $x=t\Omega$.

Fig. 5. High order Harmonic spectrum generated by focusing a high intensity (10^{14} W.cm^{-2}) 50 fs pulse of a titanium doped sapphire laser in a dense argon jet, together with its second harmonic so that both odd and even harmonics are generated.

Fig. 6. Principle of the “SPIDER” time-resolved measurement of the amplitude and phase of an ultrashort EM pulse.

Fig.7. Reshaping of Poisson-spectrum pulse (2.8) with $m=4$ and reversal of its polarity on the beam's axis in the course of propagation from $z=-2L_R$ (Fig. 7a) through $z=0$ (Fig. 7b) and further to $z=2L_R$ (Fig. 7c).

Fig. 8. Geometry of waveform-preserving reflection of a plane wave P to wave S on a parabolic reflector R : O, ρ_0 and θ are the pole, radius-vector and polar angle of the reflecting mirror R.

Fig. 9. (a) lengthening and polarity reversal due to reflection from plasma with $\alpha = 0.5$: (—□—)incident waveform $F_1(x) = L_0(x)-L_1(x)$; (—○—) reflected waveform $F_2(x)$, $x = t/t_0$. (b) Reflection of Laguerre waveform L_0 from plasma – like dielectric (normal incidence); reflection coefficient R (2.79) is plotted vs the parameter $\alpha = \Omega t_0$. (2.73).

Fig. 10. Pulse streching in a waveguide : electric strength of the pulse, observed by Mc Gowan, Gallot and Grischkowsky [1999] at the output of a span of circular waveguide (radius R=280 μm, length L=0.4 cm), is plotted vs time (2.85).

Fig. 11. Formation of a tail of reflected P-polarized *sech* pulse at the Brewster angle of incidence in the vicinity of the excitonic resonance; Calculation of the cross-correlation traces of the reflected pulse with the incident ultrashort pulse (dashed line). The values of parameters in eq. (2.71), used in calculation of these graphs, are $\varepsilon_S = 12.6$; $\beta = 4\pi 10^{-3}$; $\Omega = 55THz$; $M = nm_e$; m_e is the free electron mass. Curve 1 corresponds to an idealized model ($n\to\infty$, $\Gamma=0$). Weakening of the time-resolved reflectivity due to a finite damping factor ($n\to\infty, \Gamma= 0.8\ cm^{-1}$) or a finite electron mass ($n=0.3$, $\Gamma=0$) are shown on curves (2) and (3) respectively. Adapted from Aviskoo and Kuhl [1989]

Fig. 12. Typical variation of the reflection of thin heterogeneous film with positive dispersion. The intensity reflection coefficient $|R|^2$ is plotted vs a normalized frequency $x = \omega/\Omega_1$.

Fig. 13. Reflectivity of thin heterogeneous film with negative dispersion (2.97). The intensity reflection coefficient $|R|^2$ is plotted vs a normalized frequency $x = \omega/\Omega_2$;

Fig. 14. Time dependence of the intensity of the diffraction pattern at different diffraction angles for a pulsed source with $\gamma = 1/\omega_0 t_0 = 0.32$. The intensity is normalized to its maximum value at the center. $\beta = 2\pi(a/\lambda_0)\sin\theta$. Bertolotti, Ferrari and Sereda [1995].

Fig. 15. Exactly solvable models of normalized instantaneous dielectric susceptibility $U^2(t)$ for the equal values of $U^2_{\min} = 0.25$ and equal durations $t_c = 2t_m$; curves 1 and 2 relate to the models (3.11) and (3.31) respectively. (solid line): $U_2^2(t)$ (eq. 3.26), (dashed line): $U_1^2(t)$ (eq. 3.11)

Fig. 16. Reshaping of the leading part of harmonic cw train (ω=*1.77 rad.s*$^{-1}$) after passing through a non stationary dielectric described by the $U_1^2(t)$ temporal dependence (3.11), shown on Fig. 16 by the dashed curve. The normalized electric strength (3.16) $e = [U_1(t)]^{-3/2}\sin(q_1 z - \omega\tau)$ is plotted vs the normalized delay $(t_d - t_f)/t_c$ in a plane $z = \omega\tau(t_c)q_1^{-1}$; t_c=*4fs*, $U^2_{\min} = 0.25$

Fig. 17. Reflection coefficient of a non stationary dielectric corresponding to ε variations of eq (3.2), for different values of the parameter ϕ_0, compared to the result of a "quasistatic"

approximation using the instantaneous value of the standard Fresnel coefficient (a) Intensity reflection coefficient (b) phase. The beam is at normal incidence

Fig. 18. Modulus of reflection coefficient $|R_P|$ (Fig. 17a) and relative frequency shift $u = \Delta\omega / \omega$ (Fig. 17b) for a P-polarized wave reflected from the non-stationary dielectric $\varepsilon(t) = n_0 U^2(t)$, plotted vs the normalized time $x=t/t_m$; the model $U(t)$ is given in (3.11), $n_0=3.5$, $t_m = t_2^2 / 2t_1$. The parameters of model (3.11) are : $t_1=120\ fs$; $t_2=155\ fs$. The curves relate to several incidence angles between 60° and 75°. There is no noticeable red shift of the reflected wave for an incidence angle of 60°.

FIGURE 1

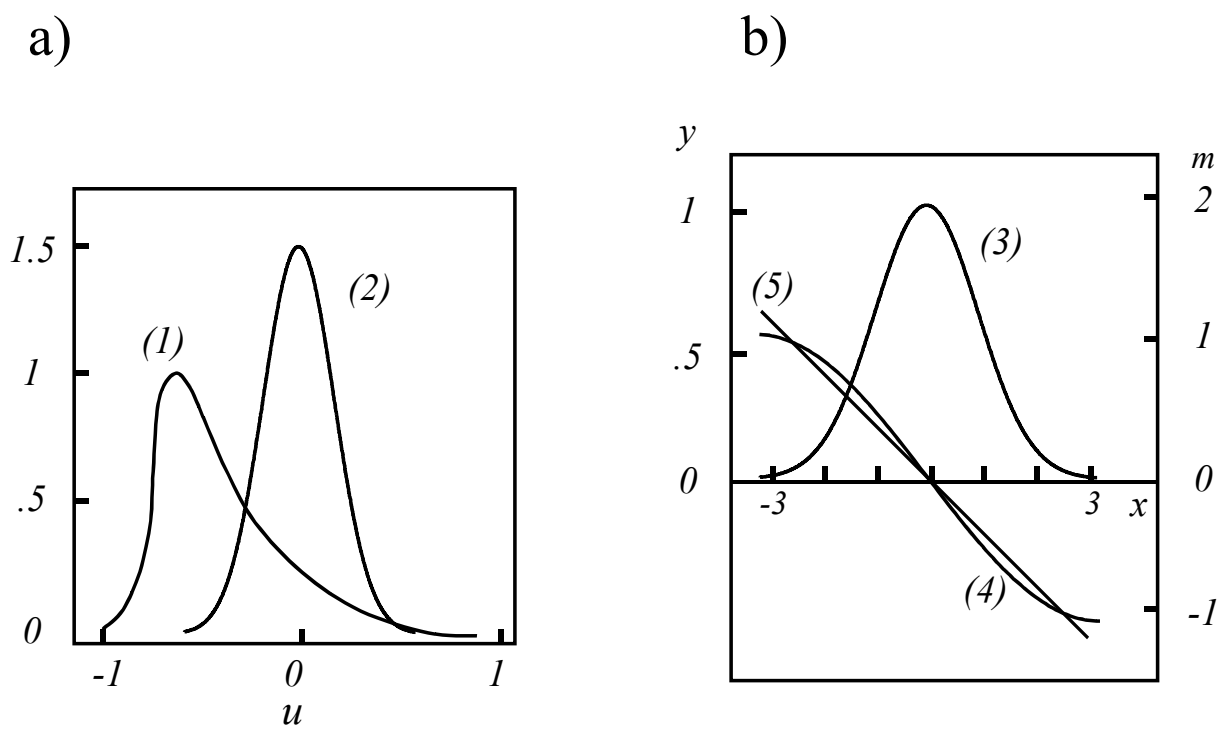

FIGURE 2

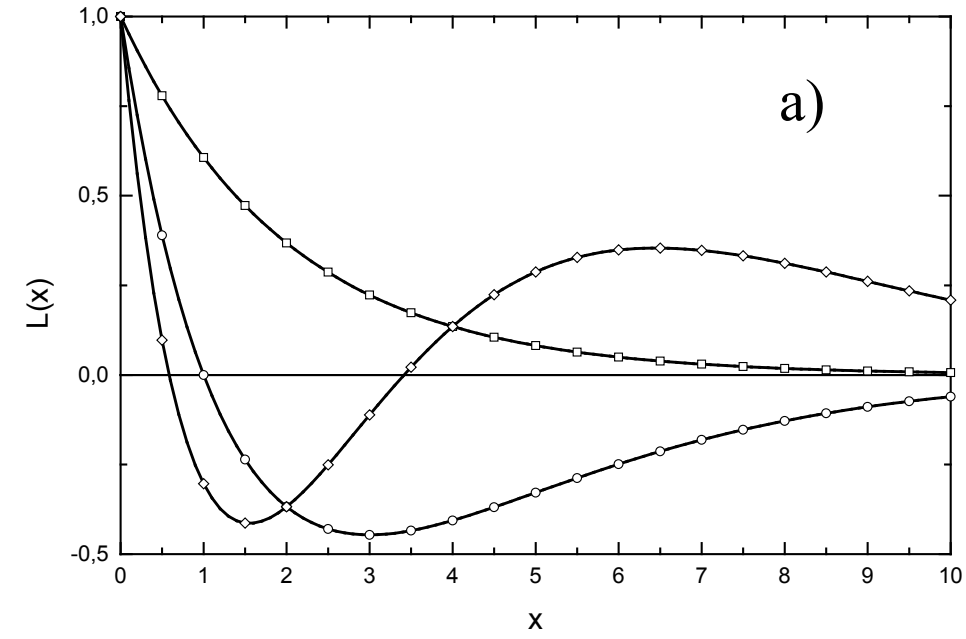
a)
L(x)
x
1,0
0,5
0,0
-0,5
0
1
2
3
4
5
6
7
8
9
10

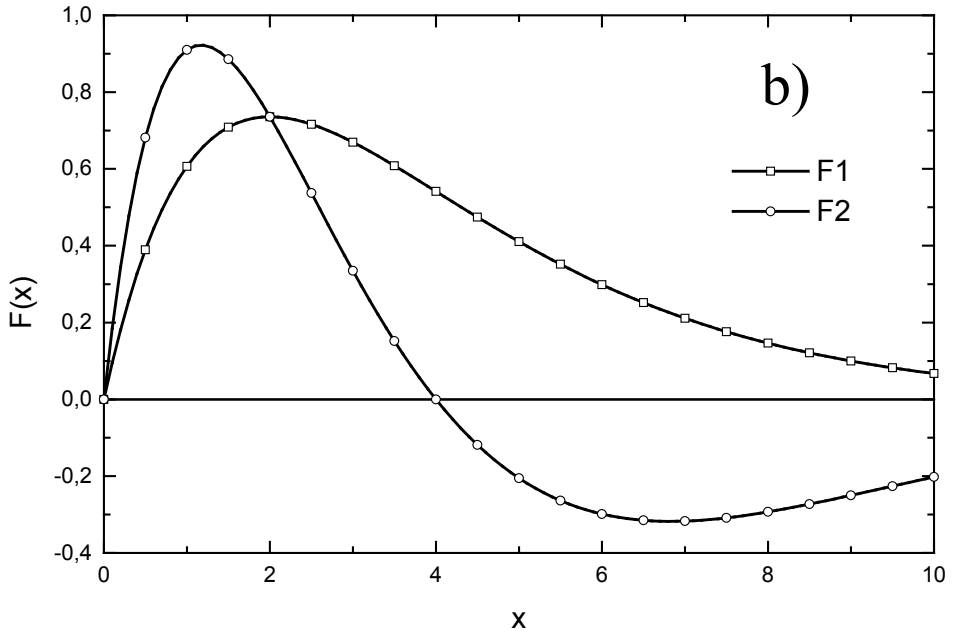
b)
F1
F2
F(x)
x
1,0
0,8
0,6
0,4
0,2
0,0
-0,2
-0,4
0
2
4
6
8
10

FIGURE 3

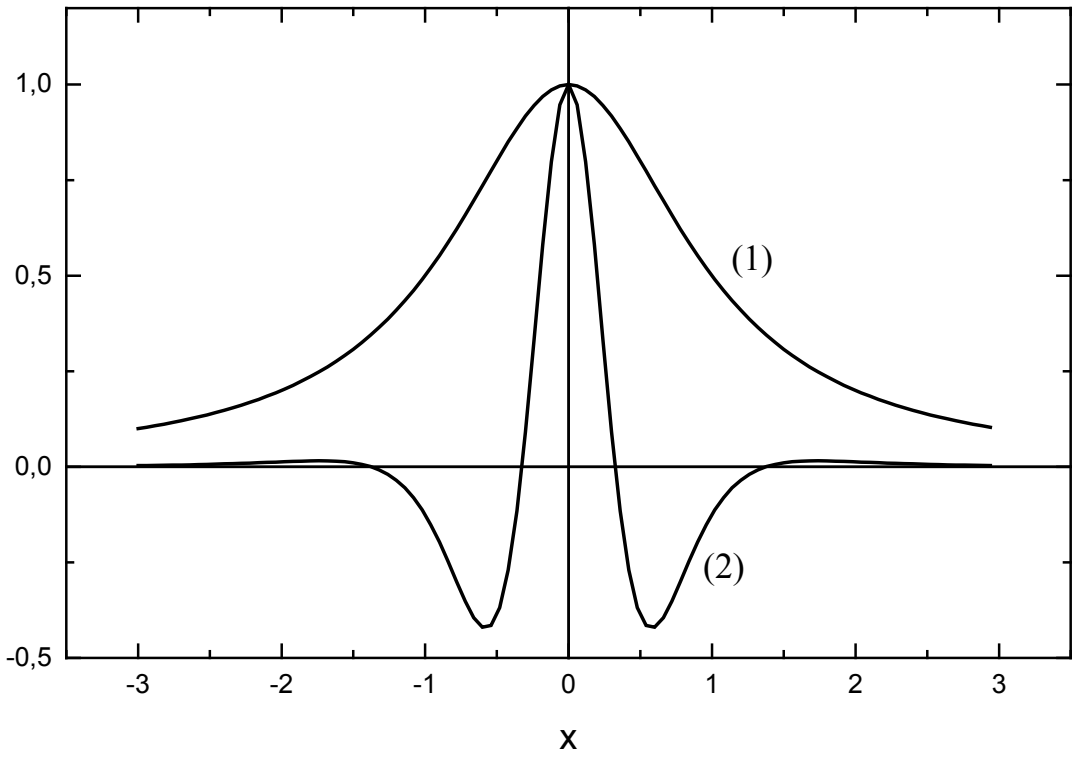

FIGURE 4

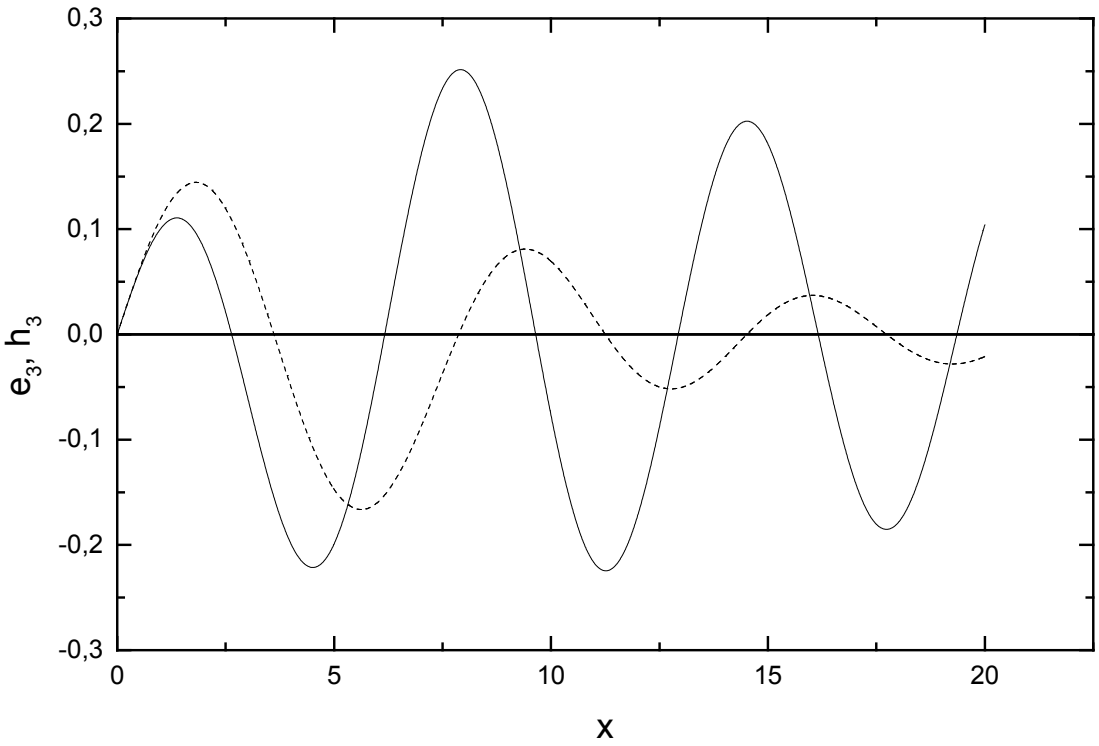

FIGURE 5

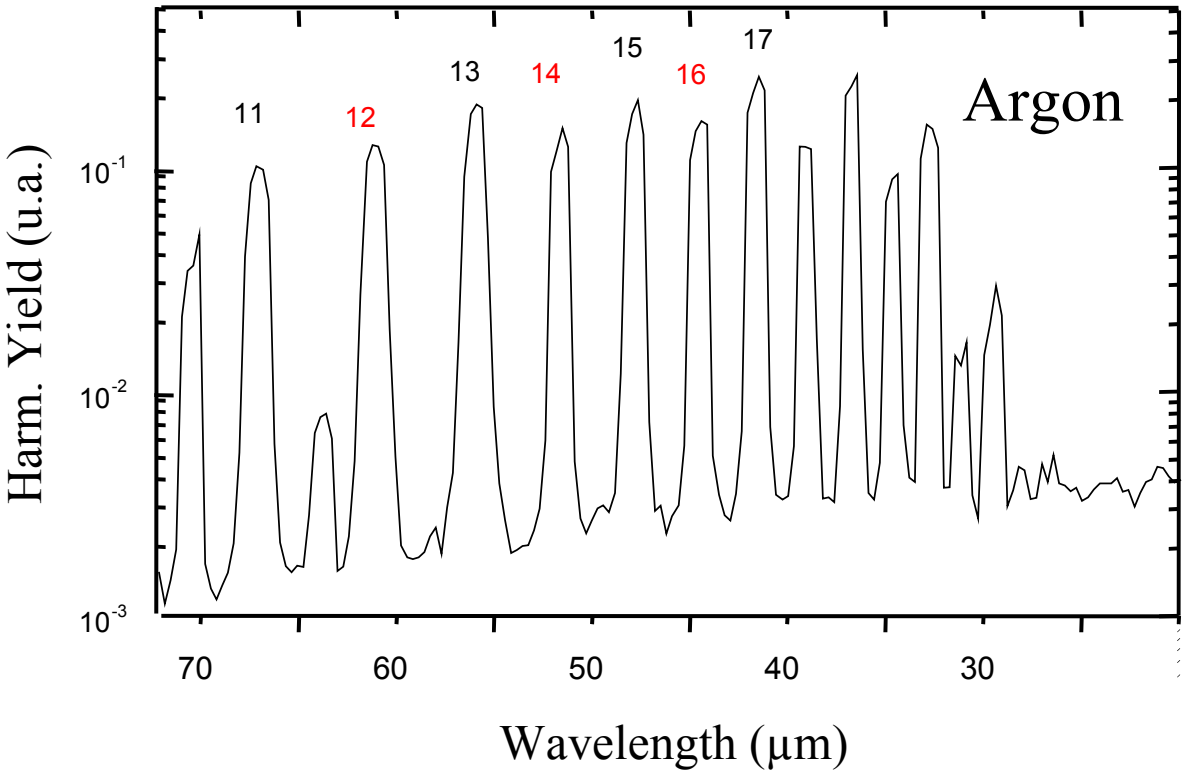
Argon
11
12
13
14
15
16
17
Harm. Yield (u.a.)
10-1
10-2
10-3
70
60
50
40
30
Wavelength (μm)

FIGURE 6

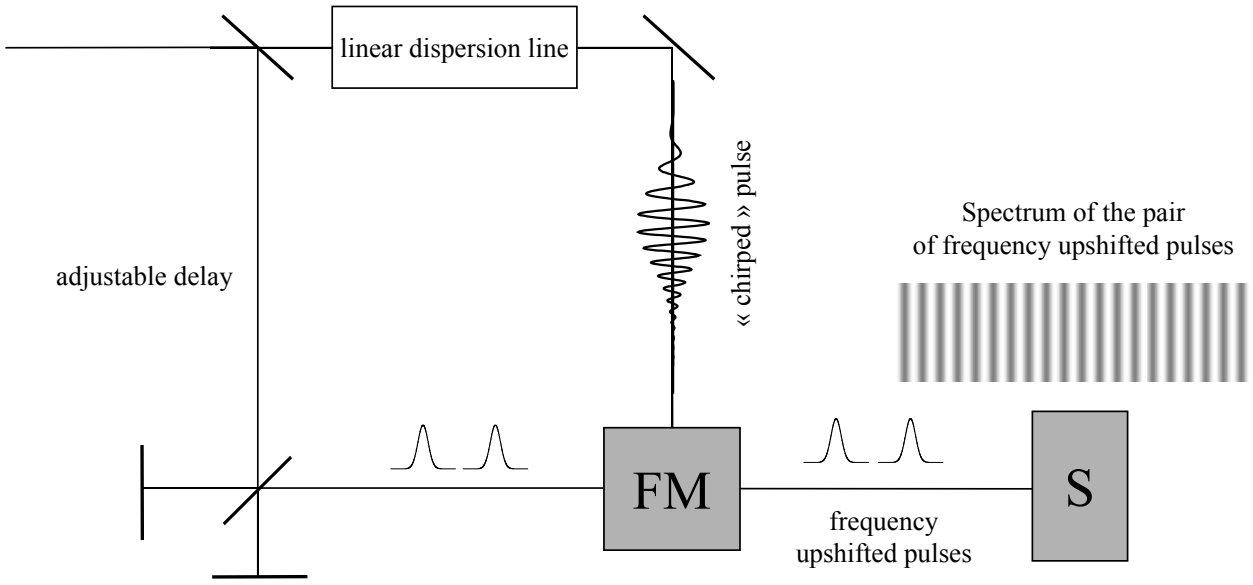
linear dispersion line
« chirped » pulse
Spectrum of the pair
of frequency upshifted pulses
adjustable delay
FM
S
frequency
upshifted pulses

FIGURE 7

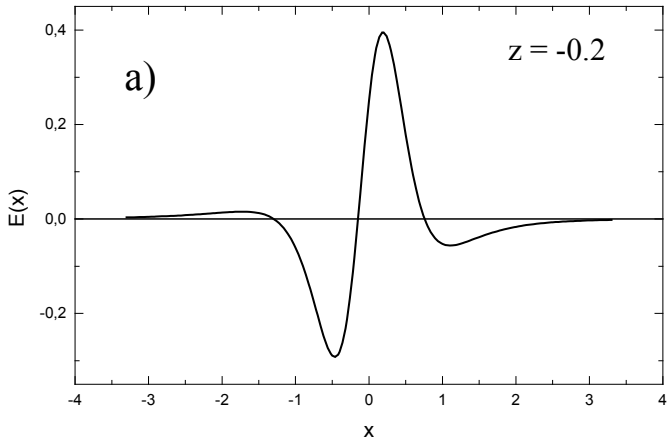
a)
z = -0.2
E(x)
x
0,4
0,2
0,0
-0,2
-4
-3
-2
-1
0
1
2
3
4

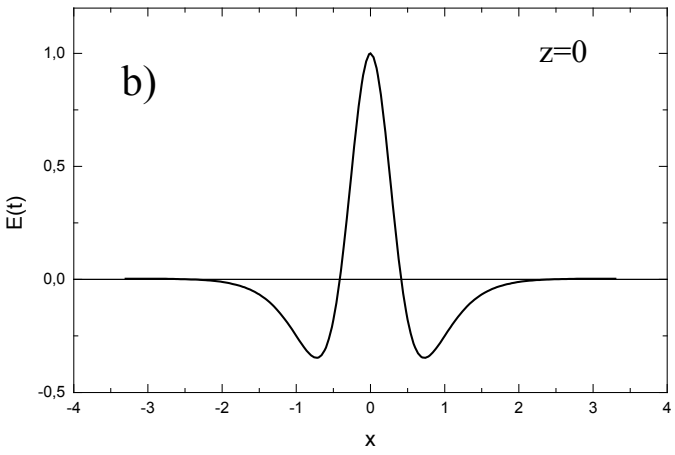
b)
z=0
E(t)
x
1,0
0,5
0,0
-0,5
-4
-3
-2
-1
0
1
2
3
4

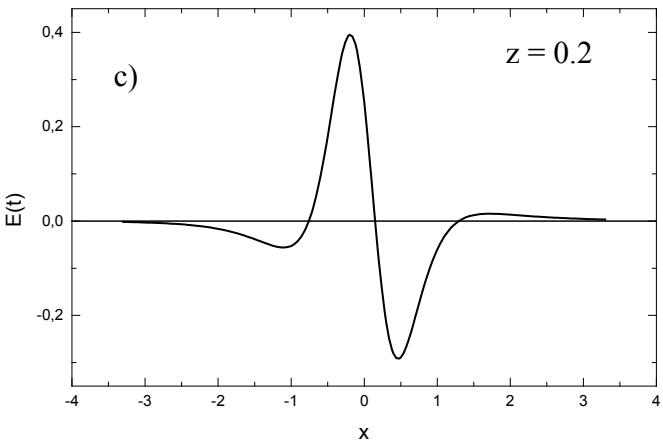
c)
z = 0.2
E(t)
x
0,4
0,2
0,0
-0,2
-4
-3
-2
-1
0
1
2
3
4

FIGURE 8

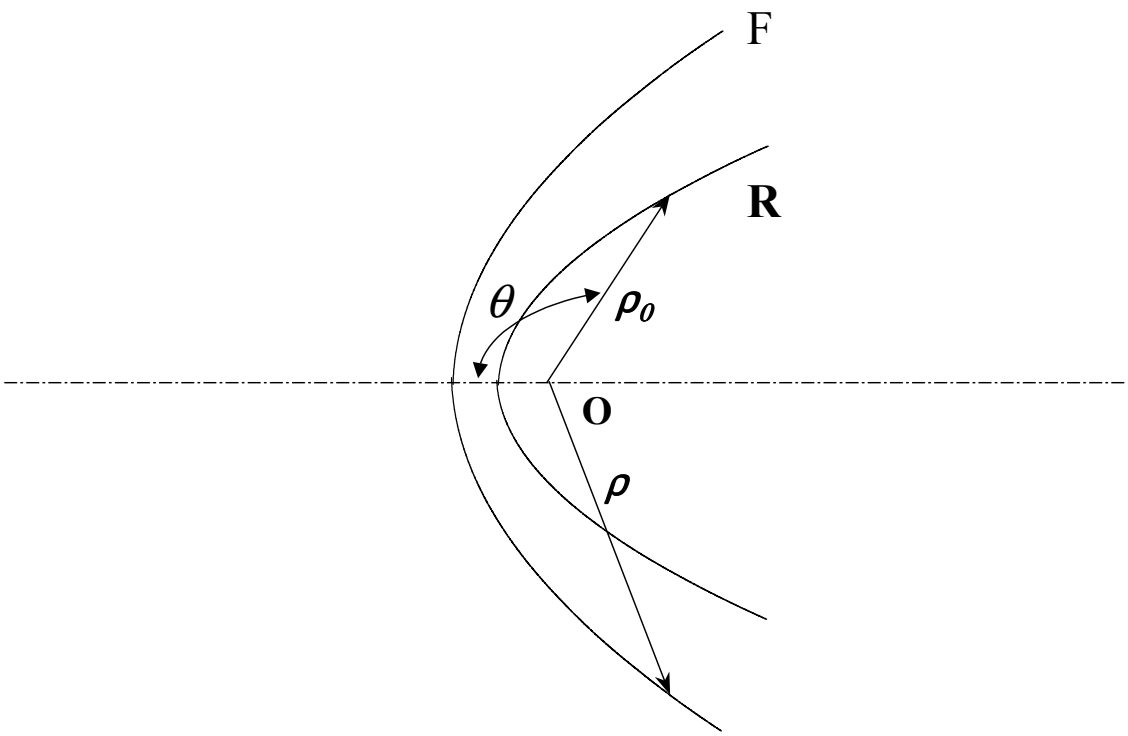

FIGURE 9

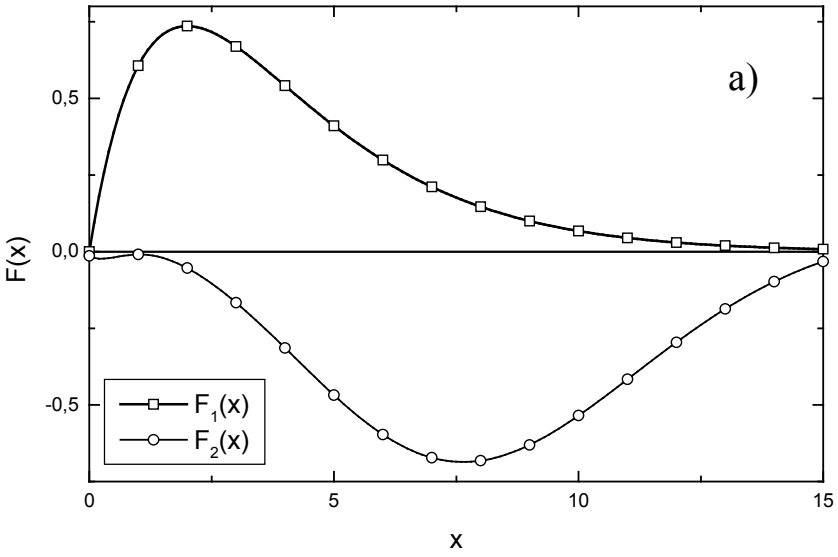

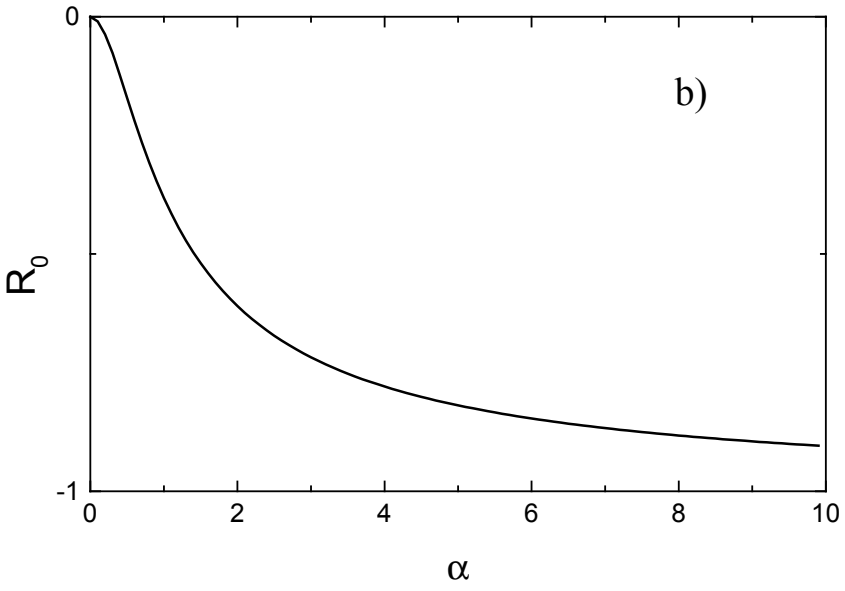

FIGURE 10

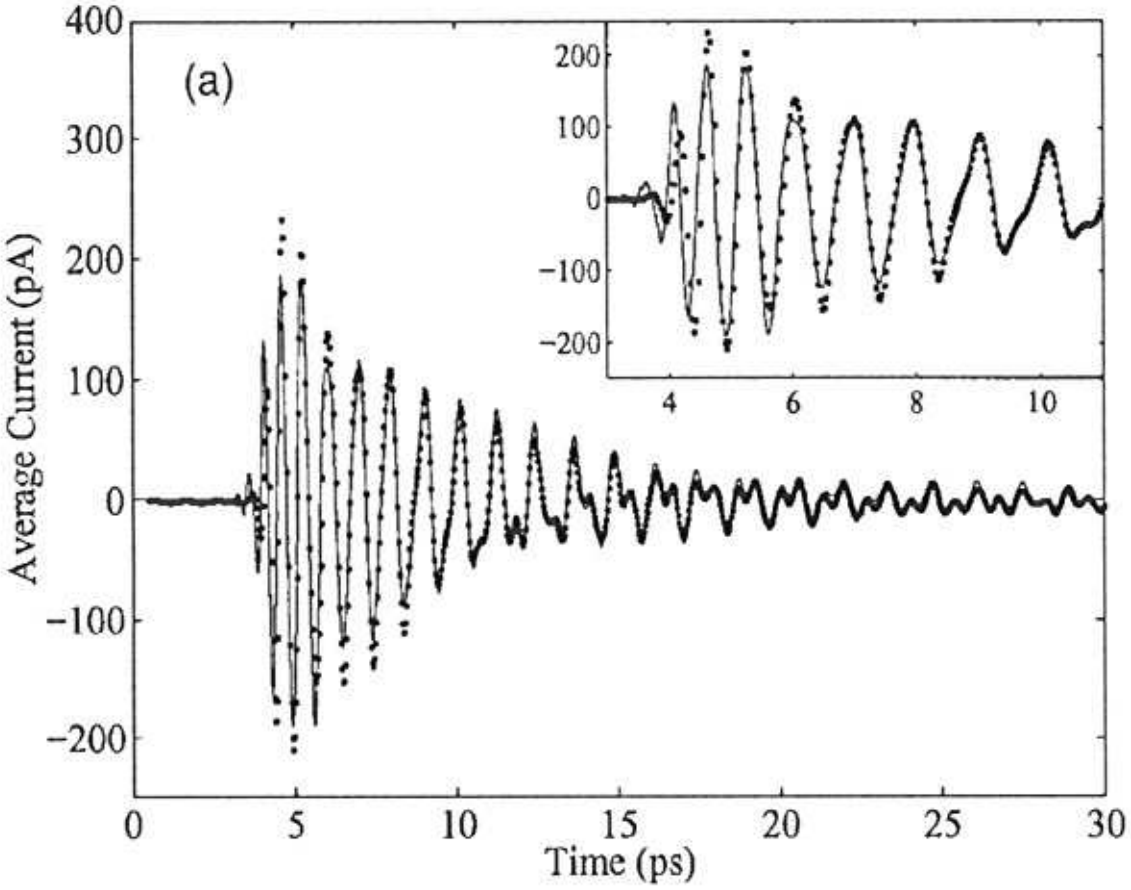
(a)
Average Current (pA)
Time (ps)
400
300
200
100
0
−100
−200
0
5
10
15
20
25
30
200
100
0
−100
−200
4
6
8
10

FIGURE 11

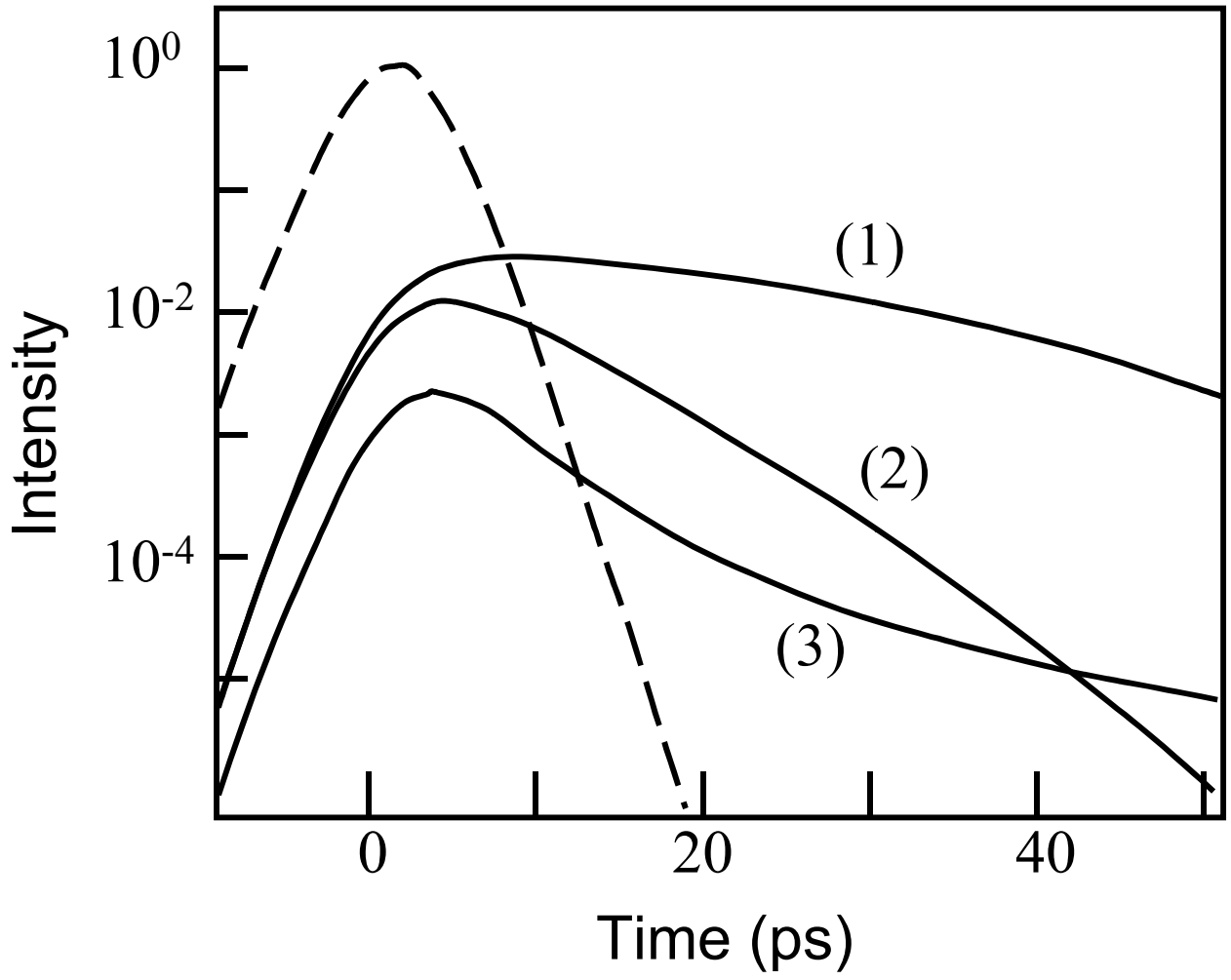

FIGURE 12

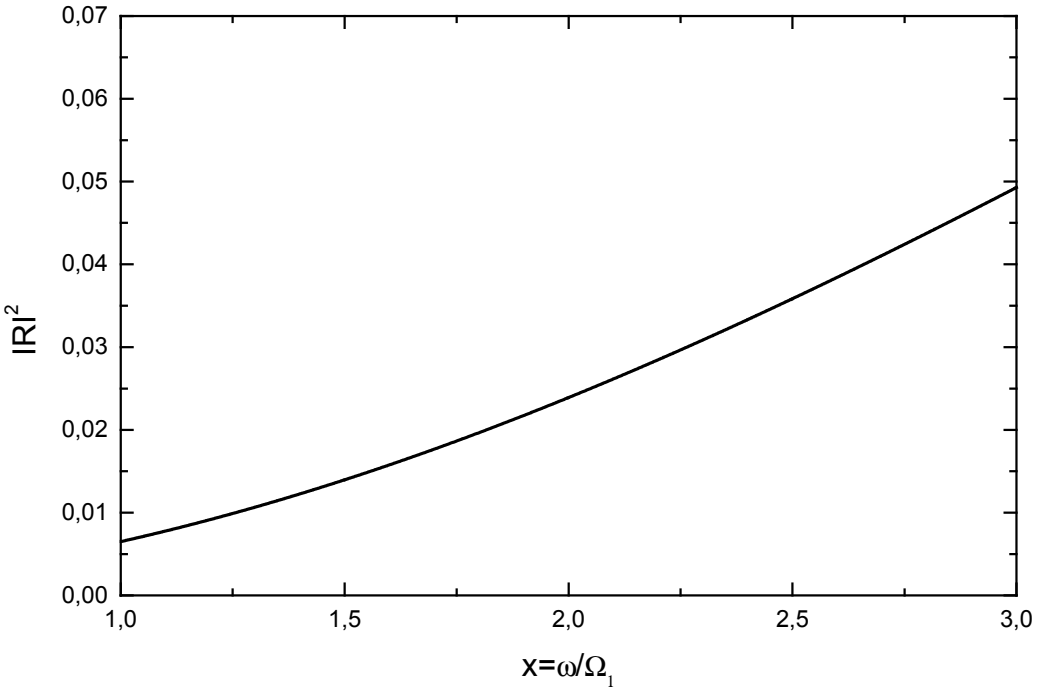

FIGURE 13

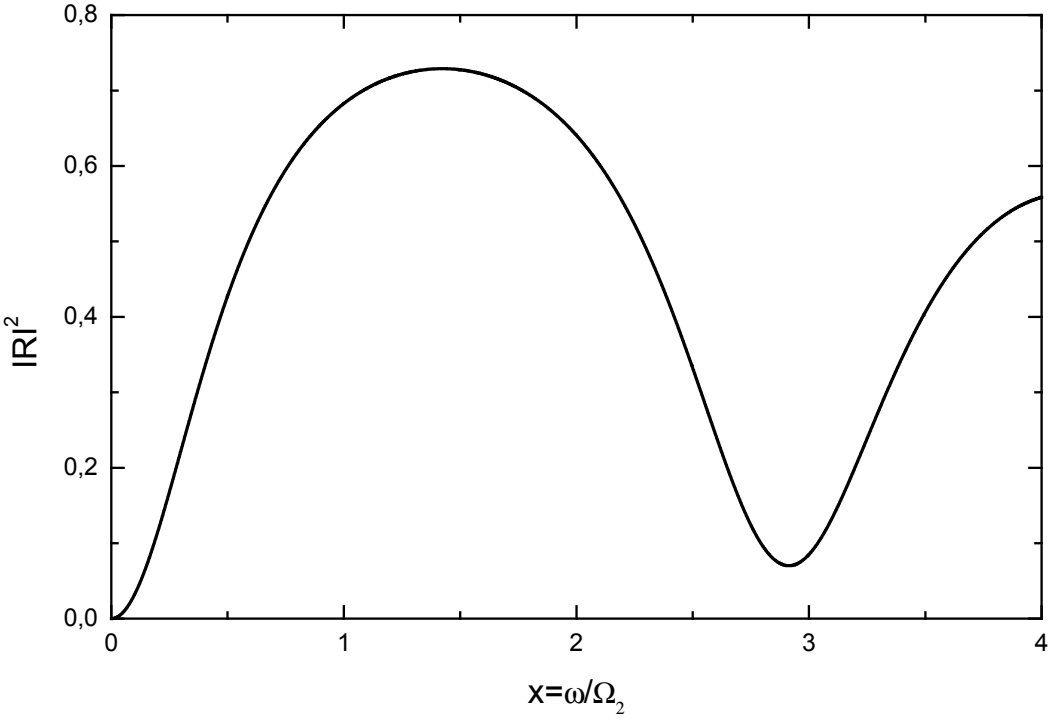

FIGURE 14

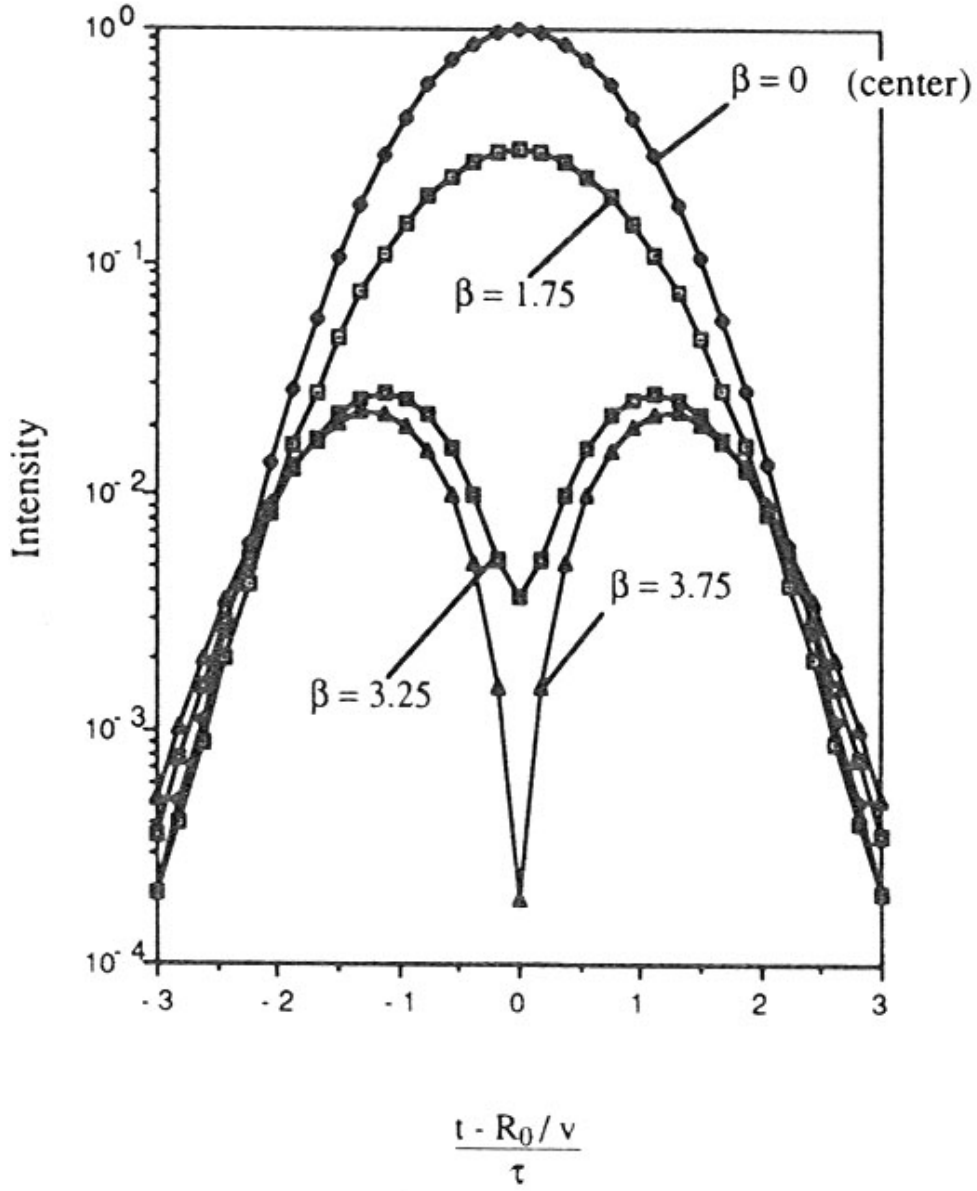
Intensity
10^0
10^{-1}
10^{-2}
10^{-3}
10^{-4}
β = 0 (center)
β = 1.75
β = 3.75
β = 3.25
-3
-2
-1
0
1
2
3
$\frac{t - R_0 / v}{\tau}$

FIGURE 15

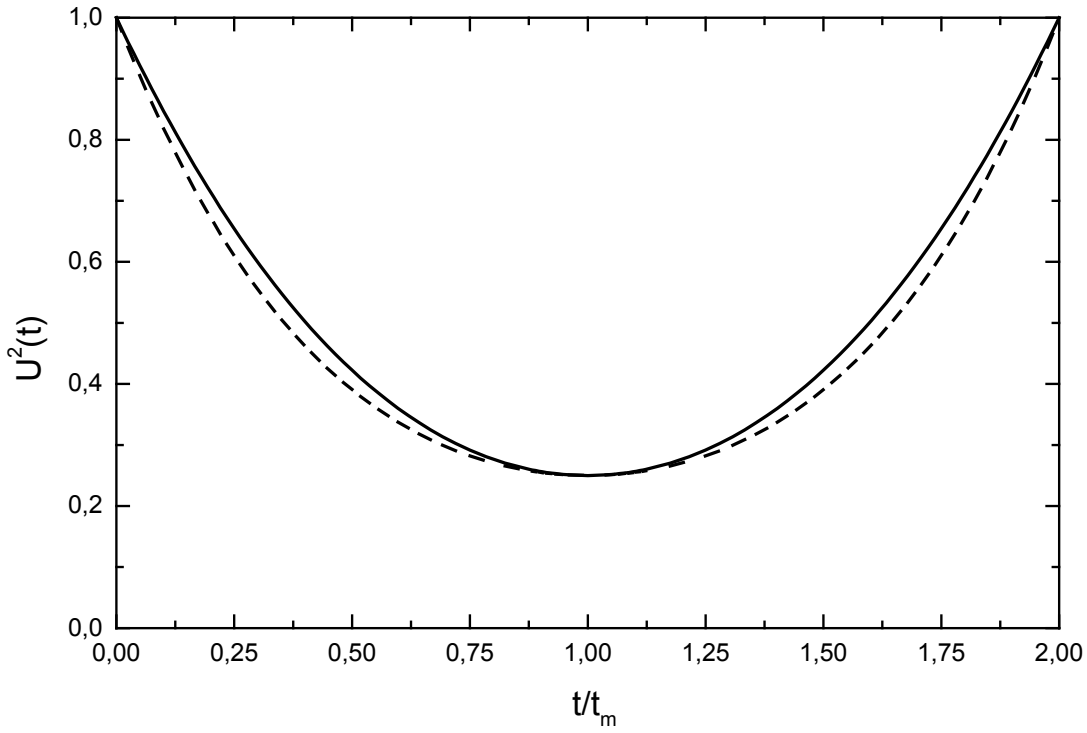

FIGURE 16

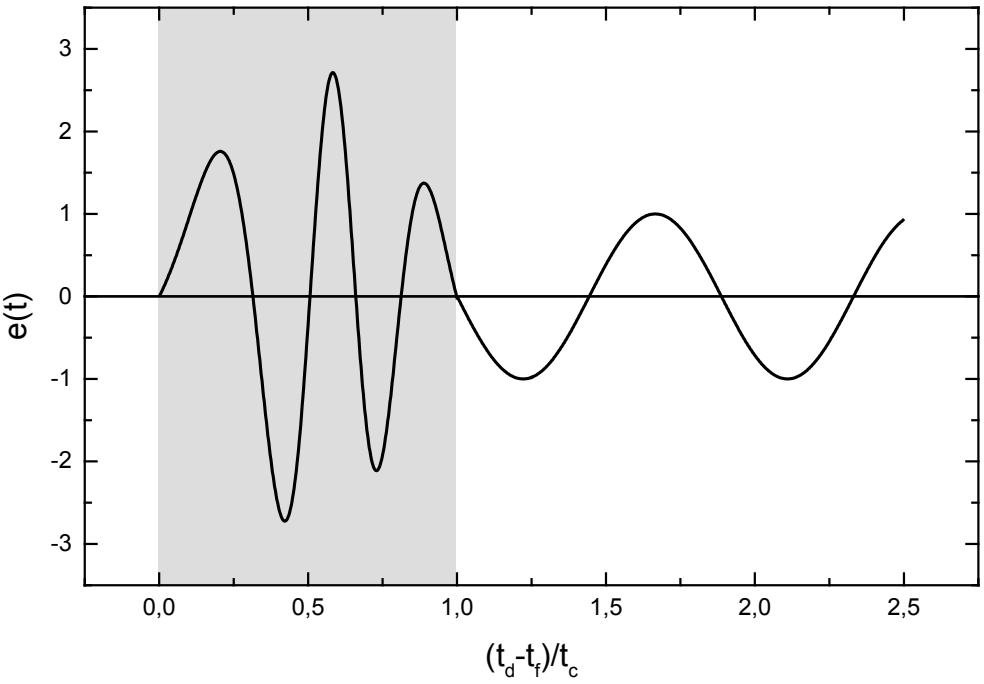

FIGURE 17

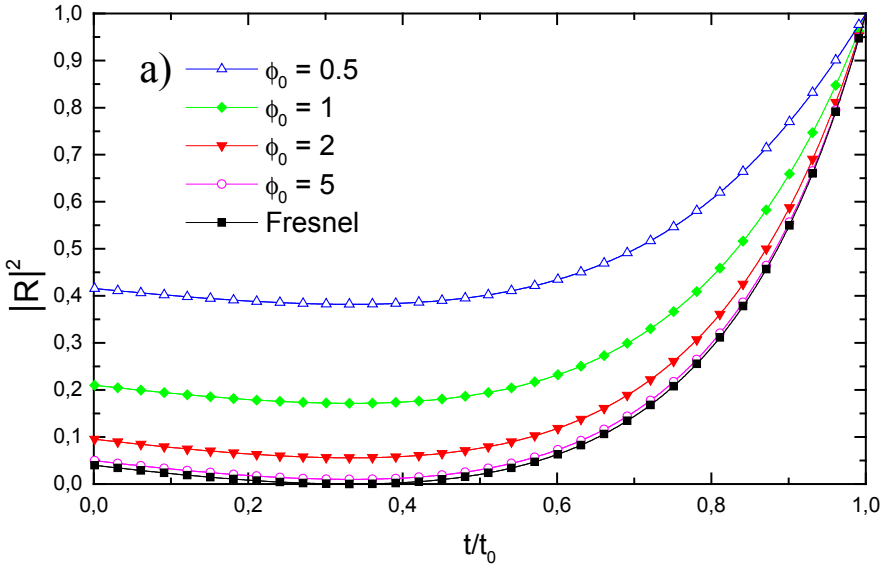
a)
ϕ_0 = 0.5
ϕ_0 = 1
ϕ_0 = 2
ϕ_0 = 5
Fresnel
$|R|^2$
t/t_0

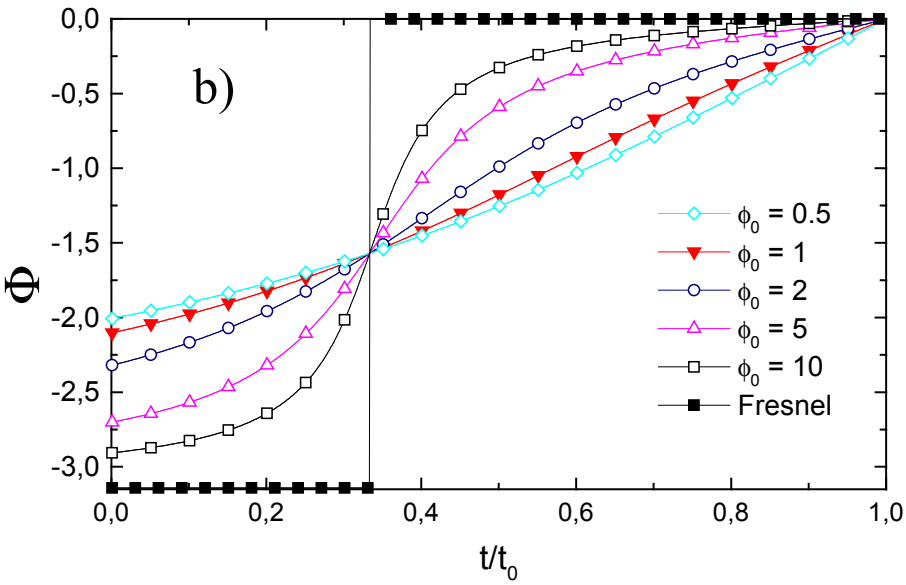
b)
ϕ_0 = 0.5
ϕ_0 = 1
ϕ_0 = 2
ϕ_0 = 5
ϕ_0 = 10
Fresnel
Φ
t/t_0

FIGURE 18

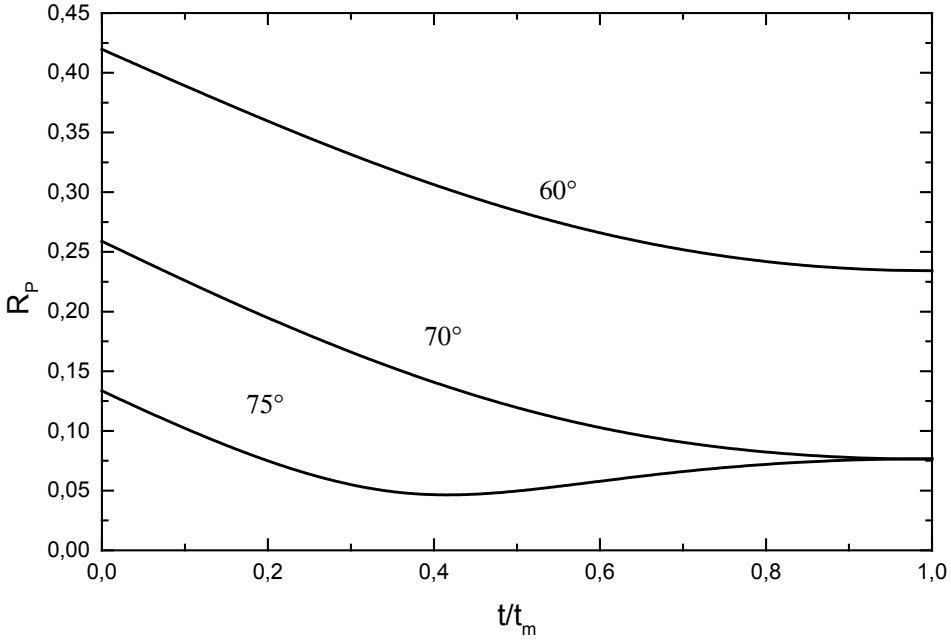
0,45
0,40
0,35
0,30
0,25
0,20
0,15
0,10
0,05
0,00
R_P
60°
70°
75°
0,0
0,2
0,4
0,6
0,8
1,0
t/t_m

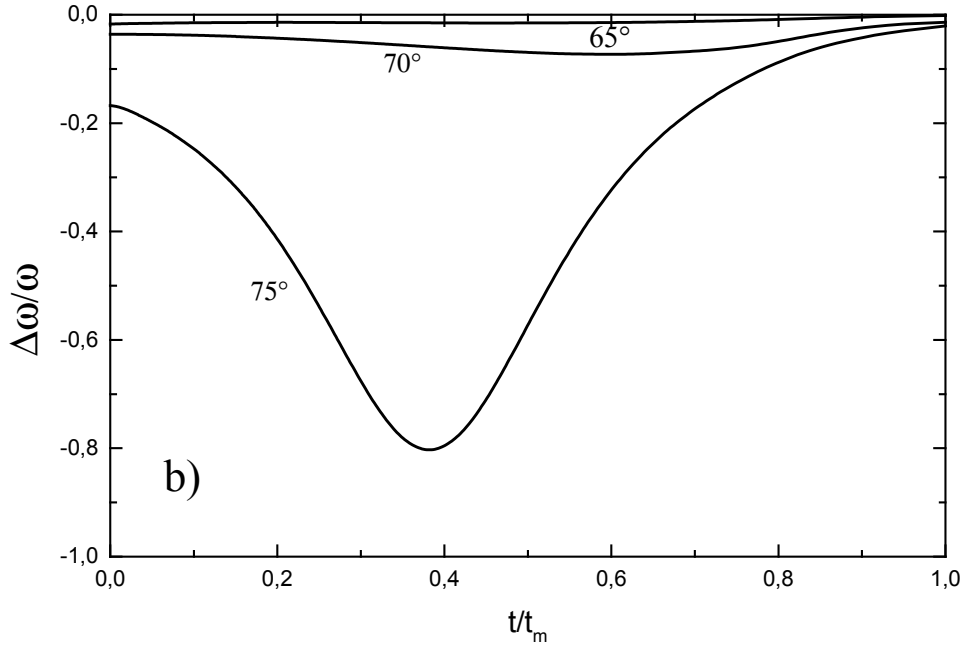
0,0
-0,2
-0,4
-0,6
-0,8
-1,0
$\Delta\omega/\omega$
65°
70°
75°
b)
0,0
0,2
0,4
0,6
0,8
1,0
t/t_m